Advances in Computational Mathematics (2023) 49:61
https://doi.org/10.1007/s10444-023-10062-y

Interior penalty discontinuous Galerkin methods for the velocity-pressure formulation of the Stokes spectral problem

Felipe Lepe[1]

Received: 16 December 2021 / Accepted: 28 June 2023 / Published online: 27 July 2023

Abstract
In this paper, we analyze discontinuous Galerkin methods based in the interior penalty method in order to approximate the eigenvalues and eigenfunctions of the Stokes eigenvalue problem. The considered methods in this work are based in discontinuous polynomials approximations for the velocity field and the pressure fluctuation in two and three dimensions. The methods under consideration are symmetric and nonsymmetric, leading to variations on the associated matrices and, hence, on the computation of the eigenvalues and eigenfunctions where real and complex results may appear, depending on the choice of the method. We derive a convergence result and error estimates for the proposed methods, together with a rigorous computational analysis of the effects of the stabilization parameter in the appearance of spurious modes when the spectrum is computed, when symmetric and nonsymmetric methods are performed.

Keywords Stokes equations · Eigenvalue problems · Discontinuous Galerkin method · Error estimates

Mathematics Subject Classification (2010) 35Q35 · 65N15 · 65N25 · 65N30 · 76D07

1 Introduction

The Stokes problem is a system of equations that describes the motion of a certain fluid. For a given domain $\Omega \subset \mathbb{R}^d$, where $d \in \{2, 3\}$ with Lipschitz boundary defined

Communicated by: Ilaria Perugia

✉ Felipe Lepe
flepe@ubiobio.cl

[1] GIMNAP-Departamento de Matemática, Universidad del Bío-Bío, Casilla 5-C, Concepción, Chile

by $\Gamma := \Gamma_D \cup \Gamma_N$, where $|\Gamma_D| > 0$, we are interested in the Stokes eigenvalue problem:

$$\begin{cases} -\nu\Delta \boldsymbol{u} + \nabla p = \lambda \boldsymbol{u} & \text{in} \quad \Omega, \\ \operatorname{div} \boldsymbol{u} = 0 & \text{in} \quad \Omega, \\ \boldsymbol{u} = \boldsymbol{0} & \text{on} \quad \Gamma_D, \\ (\nabla \boldsymbol{u} - p\mathbb{I}) \cdot \boldsymbol{n} = \boldsymbol{0} & \text{on} \quad \Gamma_N, \end{cases} \tag{1}$$

where μ is the kinematic viscosity, $\boldsymbol{u}$ is the velocity, p is the pressure, $\mathbb{I} \in \mathbb{R}^{d\times d}$ is the identity matrix, and $\boldsymbol{n}$ is the outer unit vector to Γ.

A variety of numerical methods have been developed for the Stokes eigenvalue problem due to the many applications in different contexts that require an accurate knowledge of the vibration modes of this system.

It is very well known that, one of the most important issues when the spectrum of a certain operator is approximated, is the arising of spurious eigenvalues. This pollution is important to avoid, since it has no physical meaning in real applications, motivating the development of robust and reliable numerical methods that approximate safely and accurately the eigenvalues and eigenfunctions of PDE spectral problems, in particular the one of interest on this paper.

Nowadays, it is possible to find a number of works dealing with numerical methods to approximate the solution of the Stokes spectral problem [1, 3, 11–13, 16], revealing that the research on numerical methods for the aforementioned problem is a current and important matter of study. In the present work, we contribute on this subject, with the analysis of a discontinuous Galerkin method based in the interior penalization strategy, that we will refer as IPDG.

The DG method, introduced with the spirit of solving hyperbolic problems, has shown many applications in different contexts of elliptic equations as well. A complete description of the treatment of DG methods on elliptic problems can be found in [2]. For spectral problems, the pioneer work where the DG method is considered a suitable alternative to approximate the spectrum of eigenvalue problems is [1], where the authors proved the correct approximation of the spectrum of the Laplace spectral problem, where the spurious eigenvalues are avoided, and optimal order of convergence is proved with this numerical approach. This paper has become a corner stone to solve other important eigenproblems, such as the Maxwell eigenvalue problem [3–5], elasticity spectral problem [16], and Stokes spectral problem [17], among others.

In the present paper, we continue with our research program related to the applications of DG methods for eigenvalue problems. The aforementioned references have shown interesting features to solve these type of problems, due to the flexibility for the meshes, the easy computational coding, and the accuracy on the computation of the spectrum. However, the use of DG methods, in particular the IPDG method, is important and has no minor cost: the choice of the stabilization parameter. To make matters precise, in [16, 17], the authors proved that the stability of the DG method depends on a theoretical threshold in which the stabilization parameter lies and, in the computational experiments, is relevant to localize this threshold in order to avoid the spurious eigenvalues. This choice is not arbitrary and depends on the geometrical features of the domains, boundary conditions, and physical parameters, just to mention the most important, demanding a rigorous mathematical and computational analysis

related to the stabilization parameters and the role that play on the computation of the spectrum.

Since the knowledge of the vibration modes of the Stokes eigenvalue problem is important due to the many applications in real contexts, such as the design of pipes, structures containing fluids, and fluids interacting with other fluids or structures, it is relevant to design numerical techniques to approximate the eigenvalues and eigenfunctions of the Stokes eigensystem, and DG methods are an effective alternative to compute them. With this aim, we are interested in the classic velocity/pressure formulation for the Stokes problem, which, to the best of the author's knowledge, has not been taken in consideration for the implementation of DG methods in the context of eigenvalue problems. This formulation leads to a less expensive numerical method compared with the one analyzed in [17] for a pseudostress formulation, since the presence of the aforementioned tensor obligates to approximate its corresponding components, which are more compared with the components of a vectorial formulation. This simplicity motivates the analysis of our work. However, we need to once again face the stabilization problem for the three DG methods in which our work is based: the symmetric interior penalty method (SIP), the nonsymmetric interior penalty method (NIP), and the incomplete interior penalty method (IIP). To perform the analysis of the proposed DG methods for the Stokes eigenvalue problem, we made use of the results provided in [1] for the Laplacian operator, adapting them for our case, since in the Stokes setting, the grad–grad bilinear form appears and its treatment is the same as in the aforementioned reference. The rest of the terms on the Stokes formulation can be analyzed as in the source problem. We refer to [14] for a complete treatment related to this subject.

The outline of the present paper is the following: in Sect. 2, we present the variational formulation of (1). We recall the classic properties of well posedness and regularity of the eigenfunctions, that leads us to derive the spectral characterization for the eigenvalue problem. The core of our paper is contained in Sect. 3, where we present the definitions for the elements of the mesh, averages and jumps for the functions, trace inequalities, the DG space for the velocity and piecewise polynomials for the pressure, and the discrete bilinear form that leads to the discrete eigenvalue problem which, depending on the choice of certain parameter, deliver a symmetric or nonsymmetric numerical method. We analyze the stability of the discrete formulation for the three IPDG methods under consideration. In Sect. 4, we analyze the convergence of the proposed DG method and derive error estimates, adapting the theory of non-compact operators of [6, 7]. Finally, in Sect. 5, we present a series of numerical tests in which we assess the performance of the DG methods. A rigorous analysis of the effects of the stabilization parameter in the computation of the spectrum is presented, together with a comparison between the SIP, NIP, and IIP methods. Also, we compute the eigenvalues in different domains and compute the order of convergence for each method.

1.1 Notations

Throughout this work, Ω is a generic Lipschitz bounded domain of $\mathbb{R}^2$. For $s \geq 0$, $\|\cdot\|_{s,\Omega}$ stands indistinctly for the norm of the Hilbertian Sobolev spaces $\mathrm{H}^s(\Omega)$ or

$[\mathrm{H}^s(\Omega)]^2$ with the convention $\mathrm{H}^0(\Omega) := \text{Ł}^2(\Omega)$. If X and Y are normed vector spaces, we write $X \hookrightarrow Y$ to denote that X is continuously embedded in Y. We denote by X' and $\|\cdot\|_X$ the dual and the norm of X, respectively. Finally, we employ $\mathbf{0}$ to denote a generic null vector and the relation $\mathtt{a} \lesssim \mathtt{b}$ indicates that $\mathtt{a} \leq C\mathtt{b}$, with a positive constant C which is independent of $\mathtt{a}$, $\mathtt{b}$, and the size of the elements in the mesh. The value of C might change at each occurrence. We remark that we will write the constant C only when it is needed.

2 The model problem

Let us define the following subspace of $[H^1(\Omega)]^d$ in which we will seek the velocity field $\boldsymbol{u}$

$$\boldsymbol{\mathcal{V}} := \{\boldsymbol{v} \in [H^1(\Omega)]^d \ : \ \boldsymbol{v}|_{\Gamma_D} = \mathbf{0}\}.$$

Observe that if $\Gamma = \Gamma_D$, the space $\boldsymbol{\mathcal{V}}$ is exactly the space $[H_0^1(\Omega)]^d$. The standard space for the pressure p is $\mathcal{Q} = L^2(\Omega)$ (or $L_0^2(\Omega)$ if $\Gamma = \Gamma_D$). With these spaces at hand, we introduce the following variational formulation of (1): Find $\lambda \in \mathbb{R}$ and $(\mathbf{0}, 0) \neq (\boldsymbol{u}, p) \in \boldsymbol{\mathcal{V}} \times \mathcal{Q}$ such that

$$\begin{aligned} a(\boldsymbol{u}, \boldsymbol{v}) + b(\boldsymbol{v}, p) &= \lambda(\boldsymbol{u}, \boldsymbol{v}) \ \forall\, \boldsymbol{v} \in \boldsymbol{\mathcal{V}}, \\ b(\boldsymbol{u}, q) &= 0 \qquad\quad \forall\, q \in \mathcal{Q}, \end{aligned} \tag{2}$$

where the bilinear forms $a : \boldsymbol{\mathcal{V}} \times \boldsymbol{\mathcal{V}} \to \mathbb{R}$ and $b : \boldsymbol{\mathcal{V}} \times \mathcal{Q} \to \mathbb{R}$ are defined, respectively, by

$$a(\boldsymbol{w}, \boldsymbol{v}) := \nu \int_\Omega \nabla \boldsymbol{w} : \nabla \boldsymbol{v}, \qquad b(\boldsymbol{v}, q) := -\int_\Omega q \, \mathrm{div}\, \boldsymbol{v}.$$

Now, we introduce the so-called solution operator, defined by

$$\boldsymbol{T} : \boldsymbol{\mathcal{V}} \to \boldsymbol{\mathcal{V}}, \qquad \boldsymbol{f} \mapsto \boldsymbol{T}\boldsymbol{f} := \widehat{\boldsymbol{u}},$$

where given $\boldsymbol{f} \in \boldsymbol{\mathcal{V}}$, the pair $(\widehat{\boldsymbol{u}}, \widehat{p}) \in \boldsymbol{\mathcal{V}} \times \mathcal{Q}$ solves the following source problem

$$\begin{aligned} a(\widehat{\boldsymbol{u}}, \boldsymbol{v}) + b(\boldsymbol{v}, \widehat{p}) &= (\boldsymbol{f}, \boldsymbol{v}) \ \forall\, \boldsymbol{v} \in \boldsymbol{\mathcal{V}}, \\ b(\widehat{\boldsymbol{u}}, q) &= 0 \qquad\quad \forall\, q \in \mathcal{Q}. \end{aligned} \tag{3}$$

Since problem above is well posed thanks to the Babuŝka-Brezzi theory, we conclude that $\boldsymbol{T}$ is well defined. Also, it is easy to check that $\boldsymbol{T}$ is a selfadjoint operator with respect to the L^2 inner product.

On the other hand, from [10, 21], we have the following regularity result for the Stokes spectral problem, which allows us to conclude the compactness of $\boldsymbol{T}$.

Theorem 1 *If $(\lambda, \boldsymbol{u}, p) \in \mathbb{R} \times \boldsymbol{\mathcal{V}} \times \mathcal{Q}$ solves (2), there exists $s > 0$ such that $\boldsymbol{u} \in [H^{1+s}(\Omega)]^d$ and $p \in H^s(\Omega)$.*

Remark 1 *Let us notice that if* $(\widehat{\boldsymbol{u}}, \widehat{p})$ *is the solution of* (3)*, then there exists* $s > 0$ *such that the following estimate holds (see, for instance, [18])*

$$\|\widehat{\boldsymbol{u}}\|_{1+s} + \|\widehat{p}\|_{s,\Omega} \lesssim \|\boldsymbol{f}\|_{0,\Omega}.$$

On the other hand, if $(\boldsymbol{u}, p)$ *solves the spectral problem* (2)*, then there exists* $r > 0$ *such that the following estimate holds*

$$\|\boldsymbol{u}\|_{1+r} + \|p\|_{r,\Omega} \lesssim \|\boldsymbol{u}\|_{1,\Omega}.$$

From the compactness of $\boldsymbol{T}$, it is well known that the spectrum of $\boldsymbol{T}$ satisfies $\mathrm{sp}(\boldsymbol{T}) = \{0\} \cup \{\mu_k\}_{k\in\mathbb{N}}$, where $\{\mu_k\}_{k\in\mathbb{N}}$ is a sequence of positive eigenvalues such that $\mu_k \to 0$ as $k \to +\infty$. This spectral characterization of $\boldsymbol{T}$ is a key ingredient to develop the forthcoming numerical analysis.

Let us introduce the bilinear form $A : \boldsymbol{\mathcal{W}} \times \boldsymbol{\mathcal{W}} \to \mathbb{R}$ defined by

$$A((\boldsymbol{u}, p), (\boldsymbol{v}, q)) := a(\boldsymbol{u}, \boldsymbol{v}) + b(\boldsymbol{v}, p) + b(\boldsymbol{u}, q) \quad (\boldsymbol{u}, p), (\boldsymbol{v}, q) \in \boldsymbol{\mathcal{W}},$$

where $\boldsymbol{\mathcal{W}} := \boldsymbol{\mathcal{V}} \times \mathcal{Q}$. It is clear that $A(\cdot, \cdot)$ is bounded. With this bilinear form at hand, we rewrite problem (2) as follows: Find $\lambda \in \mathbb{R}$ and $(\boldsymbol{0}, 0) \neq (\boldsymbol{u}, p) \in \boldsymbol{\mathcal{W}}$ such that

$$A((\boldsymbol{u}, p), (\boldsymbol{v}, q)) = \lambda(\boldsymbol{u}, \boldsymbol{v}) \quad \forall (\boldsymbol{v}, q) \in \boldsymbol{\mathcal{W}}. \tag{4}$$

3 The DG method

Now, our aim is to introduce the DG methods. In order to do this, we need to set some notations and definitions, inherent for these type of methods, such as DG spaces, jumps, averages, and discrete bilinear forms.

3.1 Preliminaries

Let $\mathcal{T}_h$ be a shape regular family of meshes which subdivide the domain $\bar{\Omega}$ into triangles/tetrahedra that we denote by K. Let us denote by h_K the diameter of any element $K \in \mathcal{T}_h$ and let h be the maximum of the diameters of all the elements of the mesh, i.e. $h := \max_{K\in\mathcal{T}_h}\{h_K\}$.

Let F be a closed set. We say that $F \subset \overline{\Omega}$ is an interior edge/face if F has a positive $(n-1)$-dimensional measure and if there are distinct elements K and K' such that $F = \bar{K} \cap \bar{K}'$. A closed subset $F \subset \overline{\Omega}$ is a boundary edge/face if there exists $K \in \mathcal{T}_h$ such that F is an edge/face of K and $F = \bar{K} \cap \Gamma$. Let $\mathcal{F}_h^0$ and $\mathcal{F}_h^\partial$ be the sets of interior edges/faces and boundary edges/face, respectively. We assume that the boundary mesh $\mathcal{F}_h^\partial$ is compatible with the partition $\Gamma = \Gamma_D \cup \Gamma_N$, namely,

$$\bigcup_{F\in\mathcal{F}_h^D} F = \Gamma_D \quad \text{and} \quad \bigcup_{F\in\mathcal{F}_h^N} F = \Gamma_N,$$

where $\mathcal{F}_h^D := \{F \in \mathcal{F}_h^\partial; \quad F \subset \Gamma_D\}$ and $\mathcal{F}_h^N := \{F \in \mathcal{F}_h^\partial : \quad F \subset \Gamma_N\}$. Also we denote $\mathcal{F}_h := \mathcal{F}_h^0 \cup \mathcal{F}_h^\partial$ and $\mathcal{F}_h^* := \mathcal{F}_h^0 \cup \mathcal{F}_h^N$. Also, for any element $K \in \mathcal{T}_h$, we introduce the set $\mathcal{F}(K) := \{F \in \mathcal{F}_h : \quad F \subset \partial K\}$ of edges/faces composing the boundary of K.

For any $t \geq 0$, we define the following broken Sobolev space

$$H^t(\mathcal{T}_h)^n := \{\boldsymbol{v} \in [L^2(\Omega)]^n : \quad \boldsymbol{v}|_K \in [H^t(K)]^n \quad \forall K \in \mathcal{T}_h\}.$$

Also, the space of the skeletons of the triangulations $\mathcal{T}_h$ is defined by $L^2(\mathcal{F}_h) := \prod_{F\in\mathcal{F}_h} L^2(F)$.

In the forthcoming analysis, $h_{\mathcal{F}} \in L^2(\mathcal{F}_h)$ will represent the piecewise constant function defined by $h_{\mathcal{F}}|_F := h_F$ for all $F \in \mathcal{F}_h$, where h_F denotes the diameter of edge/face F.

Let $\mathcal{P}_m(\mathcal{T}_h)$ be the space of piecewise polynomials respect with to $\mathcal{T}_h$ of degree at most $m \geq 0$; namely,

$$\mathcal{P}_m(\mathcal{T}_h) := \left\{\boldsymbol{v} \in [L^2(\Omega)]^d : v|_K \in [\mathcal{P}_m(K)]^d, \forall K \in \mathcal{T}_h\right\}.$$

Let $k \geq 1$. We define the following finite dimensional spaces:

$$\boldsymbol{\mathcal{V}}_h := \{\boldsymbol{v}_h \in [L^2(\Omega)]^d : \quad \boldsymbol{v}_h|_K \in [\mathcal{P}_k(K)]^d, \quad \forall K \in \mathcal{T}_h\},$$

and

$$\mathcal{Q}_h := \{\boldsymbol{v}_h \in L^2(\Omega) : \quad \boldsymbol{v}_h|_K \in \mathcal{P}_{k-1}(K), \quad \forall K \in \mathcal{T}_h\},$$

to approximate the velocity field and pressure, respectively.

We define averages $\{\boldsymbol{v}\} \in [L^2(\mathcal{F}_h)]^n$ and jumps $[\![\boldsymbol{v}]\!] \in L^2(\mathcal{F}_h)$ as follows

$$\{\boldsymbol{v}\}_F := (\boldsymbol{v}_K + \boldsymbol{v}_{K'})/2 \quad \text{and} \quad [\![\boldsymbol{v}]\!]\_F := \boldsymbol{v}_K \cdot \boldsymbol{n}_K + \boldsymbol{v}_{K'} \cdot \boldsymbol{n}_{K'} \quad \forall F \in \mathcal{F}(K) \cap \mathcal{F}(K'),$$

where $\boldsymbol{n}_K$ is the outward unit normal vector to ∂K and $\boldsymbol{v}_K$ represents the restriction $\boldsymbol{v}|_K$. We remark that when it is convenient, we will drop the subscript for this restriction. Also, on the boundary $\partial\Omega$ and for all $F \in \mathcal{F}(K) \cap \partial\Omega$, the averages and jumps are defined by $\{\boldsymbol{v}\}_F := \boldsymbol{v}_K$ and $[\![\boldsymbol{v}]\!]_F := \boldsymbol{v}_K \cdot \boldsymbol{n}$, respectively.

Inspired by the analysis of [1], let us define $\boldsymbol{\mathcal{V}}(h) := \boldsymbol{\mathcal{V}} + \boldsymbol{\mathcal{V}}_h$ which we endow with the following norm

$$\|\boldsymbol{v}\|^2_{\boldsymbol{\mathcal{V}}(h)} = \|\nabla_h \boldsymbol{v}\|^2_{0,\Omega} + \|h^{-1/2}[\![\boldsymbol{v}]\!]\|^2_{0,\mathcal{F}_h},$$

which coincides with the natural norm of $\boldsymbol{\mathcal{V}}$.

Motivated by the DG discretization for the Laplace eigenvalue problem of [1], we introduce the following property: there exists a positive constant C, depending only on the domain, such that for every $\boldsymbol{\tau} \in \boldsymbol{\mathcal{V}}(h)$, there holds

$$\|\boldsymbol{\tau}\|_{0,\Omega} \lesssim \|\boldsymbol{\tau}\|_{\boldsymbol{\mathcal{V}}(h)}. \tag{5}$$

Observe that this property is the DG version for the classic Poincaré inequality. Finally, we introduce the following trace inequality (see [8]):

$$\|h^{1/2}\{v_K\}\|_{0,\mathcal{F}} \lesssim \|v\|_{0,\Omega} \quad \forall v \in \mathcal{P}_k(\mathcal{T}_h). \tag{6}$$

3.2 Symmetric and nonsymmetric DG schemes

With the discrete spaces defined previously, we introduce the discrete counterpart of (2) as follows: Find $\lambda_h \in \mathbb{C}$ and $(\mathbf{0}, 0) \neq (\boldsymbol{u}_h, p_h) \in \boldsymbol{\mathcal{V}}_h \times \mathcal{Q}_h$ such that

$$\begin{aligned} a_h(\boldsymbol{u}_h, \boldsymbol{v}_h) + b_h(\boldsymbol{v}_h, p_h) &= \lambda_h(\boldsymbol{u}_h, \boldsymbol{v}_h) \ \forall\, \boldsymbol{v}_h \in \boldsymbol{\mathcal{V}}_h, \\ b_h(\boldsymbol{u}_h, q_h) &= 0 \qquad\qquad \forall\, q_h \in \mathcal{Q}_h, \end{aligned} \tag{7}$$

where the bilinear form $a_h : \boldsymbol{\mathcal{V}}_h \times \boldsymbol{\mathcal{V}}_h \to \mathbb{C}$ is defined by

$$\begin{aligned} a_h(\boldsymbol{u}_h, \boldsymbol{v}_h) := \int_\Omega \nu \nabla_h \boldsymbol{u}_h : \nabla_h \boldsymbol{v}_h + \int_{\mathcal{F}_h^*} \frac{\mathtt{a}_S}{h_{\mathcal{F}}} \nu [\![\boldsymbol{u}_h]\!] \cdot [\![\boldsymbol{v}_h]\!] \\ - \int_{\mathcal{F}_h^*} \{\nu \nabla_h \boldsymbol{u}_h\} \cdot [\![\boldsymbol{v}_h]\!] \\ - \varepsilon \int_{\mathcal{F}_h^*} \{\nu \nabla_h \boldsymbol{v}_h\} \cdot [\![\boldsymbol{u}_h]\!], \end{aligned} \tag{8}$$

where $\mathtt{a}_S > 0$ is a positive constant which we will refer as the stabilization parameter and $\varepsilon \in \{-1, 0, 1\}$. It is easy to check that $a_h(\cdot, \cdot)$ is a bounded bilinear form. Indeed, for $\boldsymbol{u}_h, \boldsymbol{v}_h \in \boldsymbol{\mathcal{V}}_h$, we have

$$\begin{aligned} |a_h(\boldsymbol{u}_h, \boldsymbol{v}_h)| &\leq \nu \|\nabla_h \boldsymbol{u}_h\|_{0,\Omega} \|\nabla_h \boldsymbol{v}_h\|_{0,\Omega} + \mathtt{a}_S \nu \|h_{\mathcal{F}}^{-1/2} [\![\boldsymbol{u}_h]\!]\|_{0,\mathcal{F}_h^*} \|h_{\mathcal{F}}^{-1/2} [\![\boldsymbol{v}_h]\!]\|_{0,\mathcal{F}_h^*} \\ &\quad + \nu \|h_{\mathcal{F}}^{1/2} \{\nabla_h \boldsymbol{u}_h\}\|_{0,\mathcal{F}_h^*} \|h_{\mathcal{F}}^{-1/2} [\![\boldsymbol{v}_h]\!]\|_{0,\mathcal{F}_h^*} \\ &\quad + \varepsilon \|h_{\mathcal{F}}^{1/2} \{\nabla_h \boldsymbol{v}_h\}\|_{0,\mathcal{F}_h^*} \|h_{\mathcal{F}}^{-1/2} [\![\boldsymbol{u}_h]\!]\|_{0,\mathcal{F}_h^*} \\ &\leq \underbrace{C \max\{\nu, \mathtt{a}_S \nu, \varepsilon\}}_{:= M_{DG}} \|(\boldsymbol{u}_h, p_h)\|_{\boldsymbol{\mathcal{V}}(h) \times \mathcal{Q}} \|(\boldsymbol{v}_h, q_h)\|_{\boldsymbol{\mathcal{V}}(h) \times \mathcal{Q}}, \end{aligned}$$

where C is the constant of (6).

On the other hand, we define the bounded bilinear form $b_h : \boldsymbol{\mathcal{V}}_h \times \mathcal{Q}_h \to \mathbb{C}$ by

$$b_h(\boldsymbol{v}_h, q_h) := -\int_\Omega \operatorname{div}_h \boldsymbol{v}_h q_h + \int_{\mathcal{F}_h^*} \{q_h\} [\![\boldsymbol{v}_h]\!], \quad \forall \boldsymbol{v} \in \boldsymbol{\mathcal{V}}_h, \ \forall q_h \in \mathcal{Q}_h.$$

Now, and similar to the continuous case, we rewrite (7) as follows: Find $\lambda_h \in \mathbb{C}$ and $(\boldsymbol{u}_h, p_h) \in \boldsymbol{\mathcal{W}}_h := \boldsymbol{\mathcal{V}}_h \times \mathcal{Q}_h$ such that

$$A_h((\boldsymbol{u}_h, p_h), (\boldsymbol{v}_h, q_h)) = \lambda_h(\boldsymbol{u}_h, \boldsymbol{v}_h) \quad \forall (\boldsymbol{v}_h, q_h) \in \boldsymbol{\mathcal{W}}_h,$$

where

$$A_h((\boldsymbol{u}_h, p_h), (\boldsymbol{v}_h, q_h)) := a_h(\boldsymbol{u}_h, \boldsymbol{v}_h) + b_h(\boldsymbol{v}_h, p_h) + b_h(\boldsymbol{u}_h, q_h),$$

for all $(\boldsymbol{u}_h, p_h), (\boldsymbol{v}_h, q_h) \in \boldsymbol{\mathcal{W}}_h$. Observe that $A_h(\cdot, \cdot)$ is a bounded bilinear form due the boundedness of $a_h(\cdot, \cdot)$ and $b_h(\cdot, \cdot)$.

In the definition of $a_h(\cdot, \cdot)$, the constant $\varepsilon \in \{-1, 0, 1\}$ is the parameter that dictates if the DG method is symmetric or nonsymmetric. More precisely, if $\varepsilon = 1$, we obtain the classic symmetric interior penalty method (SIP) as the one studied, for example, in [16] for the elasticity eigenproblem. If $\varepsilon = -1$, we obtain the nonsymmetric interior penalty method (NIP) and if $\varepsilon = 0$ the incomplete interior penalty method (IIP). Clearly, when nonsymmetric methods are considered, complex computed eigenvalues are expected when the spectrum is approximated.

Let us remark that the SIP method is relevant since it yields to optimal order of convergence for the approximation of the eigenvalues and eigenfunctions, whereas the NIP and IIP methods deliver suboptimal orders. This will be observed in the numerical section.

Now, the IPDG discretization of (4) reads as follows: Find $\lambda \in \mathbb{C}$ and $(\boldsymbol{u}_h, p_h) \in \boldsymbol{\mathcal{W}}_h$ such that

$$A_h((\boldsymbol{u}_h, p_h), (\boldsymbol{v}_h, q_h)) = \lambda_h(\boldsymbol{u}_h, \boldsymbol{v}_h) \quad \forall (\boldsymbol{v}_h, q_h) \in \boldsymbol{\mathcal{W}}_h.$$

To establish the well posedness of our discrete problem (7), we have from [14, Proposition 10] the following discrete inf-sup condition

$$\sup_{\boldsymbol{\tau}_h \in \boldsymbol{\mathcal{V}}_h} \frac{b_h(\boldsymbol{\tau}_h, q_h)}{\|\boldsymbol{\tau}_h\|_{\boldsymbol{\mathcal{V}}(h)}} \geq \beta \|q_h\|_{0,\Omega} \quad \forall q_h \in \mathcal{Q}_h,$$

where the constant $\beta > 0$ is independent of h. On the other hand, let us define the discrete kernel $\boldsymbol{\mathcal{K}}_h$ of $b_h(\cdot, \cdot)$ as follows:

$$\boldsymbol{\mathcal{K}}_h := \{\boldsymbol{\tau}_h \in \boldsymbol{\mathcal{V}}_h \,:\, b_h(\boldsymbol{\tau}_h, \boldsymbol{v}_h) = 0 \quad \forall \boldsymbol{v}_h \in \boldsymbol{\mathcal{V}}_h\}.$$

With this space at hand, we prove the following coercivity result for $a_h(\cdot, \cdot)$.

Lemma 1 *[ellipticity of $a_h(\cdot, \cdot)$] For any $\varepsilon \in \{-1, 0, 1\}$, there exists a positive parameter a^* such that for all $a_S \geq a^*$ there holds*

$$a_h(\boldsymbol{v}_h, \boldsymbol{v}_h) \geq \alpha \|\boldsymbol{v}_h\|^2_{\boldsymbol{\mathcal{V}}(h)} \quad \forall \boldsymbol{v}_h \in \boldsymbol{\mathcal{K}}_h,$$

where $\alpha > 0$ is independent of h.

Proof Let $\boldsymbol{v}_h \in \mathcal{K}_h$. Then, from the definition of $a_h(\cdot,\cdot)$, considering the well known inequality $ab \le \frac{a^2}{2\eta} + \frac{\eta b^2}{2}$, for all $\eta > 0$, and (6), we have

$$
\begin{aligned}
a_h(\boldsymbol{v}_h, \boldsymbol{v}_h) := \int_\Omega \nu \nabla_h \boldsymbol{v}_h : \nabla_h \boldsymbol{v}_h + \int_{\mathcal{F}_h^*} \frac{\mathtt{a}_S}{h_{\mathcal{F}}} \nu [\![\boldsymbol{v}_h]\!] \cdot [\![\boldsymbol{v}_h]\!] \\
- \int_{\mathcal{F}_h^*} \{\nu \nabla_h \boldsymbol{v}_h\} \cdot [\![\boldsymbol{v}_h]\!] \\
- \varepsilon \int_{\mathcal{F}_h^*} \{\nu \nabla_h \boldsymbol{v}_h\} \cdot [\![\boldsymbol{v}_h]\!] \\
\ge \nu \|\nabla_h \boldsymbol{v}_h\|_{0,\Omega}^2 + \mathtt{a}_S \nu \|h_{\mathcal{F}}^{-1/2} [\![\boldsymbol{v}_h]\!]\|_{0,\mathcal{F}_h^*}^2 - \nu(1+\varepsilon) \int_{\mathcal{F}_h^*} \{\nabla_h \boldsymbol{v}_h\} \cdot [\![\boldsymbol{v}_h]\!] \\
\ge \nu \|\nabla_h \boldsymbol{v}_h\|_{0,\Omega}^2 + \mathtt{a}_S \nu \|h_{\mathcal{F}}^{-1/2} [\![\boldsymbol{v}_h]\!]\|_{0,\mathcal{F}_h^*}^2 \\
+ \nu(1+\varepsilon) \left(- \frac{\|h_{\mathcal{F}}^{1/2} \{\nabla_h \boldsymbol{v}_h\}\|_{0,\mathcal{F}_h^*}^2}{2\eta} - \frac{\eta \|h_{\mathcal{F}}^{-1/2} [\![\boldsymbol{v}_h]\!]\|_{0,\mathcal{F}_h^*}^2}{2} \right) \\
\ge \nu \underbrace{\left(1 - C\frac{(1+\varepsilon)}{2\eta}\right)}_{C_1} \|\nabla_h \boldsymbol{v}_h\|_{0,\Omega}^2 + \nu \underbrace{\left(\mathtt{a}_S - \frac{\eta(1+\varepsilon)}{2}\right)}_{C_2} \|h_{\mathcal{F}}^{-1/2} [\![\boldsymbol{v}_h]\!]\|_{0,\mathcal{F}_h^*}^2,
\end{aligned}
$$

where the constant C is the one provided by (6). Observe that $C_1 > 0$ if and only if η is chosen as $\eta > (1+\varepsilon)C/2$. Now, the ellipticity holds for $\alpha := \nu \min\{C_1, C_2\}$ and choosing $\mathtt{a}_S$ such that $\mathtt{a}_S > \mathtt{a}^* := (1+\varepsilon)\eta/2$, where η has been previously determined. This concludes the proof. □

As a consequence of lemma above, it is easy to check that

$$
A_h((\boldsymbol{v}_h, q_h); (\boldsymbol{v}_h, q_h)) \ge \alpha \|\boldsymbol{v}_h\|_{\boldsymbol{\mathcal{V}}(h)}^2 \quad \forall \boldsymbol{v}_h \in \mathcal{K}_h. \tag{9}
$$

Let us introduce the discrete solution operator defined by

$$
\boldsymbol{T}_h : \boldsymbol{\mathcal{V}} \to \boldsymbol{\mathcal{V}}_h, \qquad \boldsymbol{f} \mapsto \boldsymbol{T}_h \boldsymbol{f} := \widehat{\boldsymbol{u}}_h,
$$

where given $\boldsymbol{f} \in \boldsymbol{\mathcal{V}}$, the pair $(\widehat{\boldsymbol{u}}_h, \widehat{p}_h) \in \boldsymbol{\mathcal{W}}_h$ solves the following discrete source problem

$$
A_h((\widehat{\boldsymbol{u}}_h, \widehat{p}_h), (\boldsymbol{v}_h, q_h)) = (\boldsymbol{f}, \boldsymbol{v}_h) \quad \forall (\boldsymbol{v}_h, q_h) \in \boldsymbol{\mathcal{W}}_h.
$$

4 Convergence and error estimates

The aim of this section is to derive convergence results and error estimates for our DG methods. Despite the fact that $\boldsymbol{T}$ is compact, the classic theory of compact operators is not enough to conclude the convergence in norm between the continuous and discrete

solution operators, since the numerical method of our interest is non-conforming. Is this reason, and following the spirit of [1], why we resort to the theory of non-compact operators of [6, 7]?

In what follows, we will denote by $\|\cdot\|_{\mathcal{L}(\boldsymbol{\mathcal{V}}(h),\boldsymbol{\mathcal{V}}(h))}$ the corresponding norm acting from $\boldsymbol{\mathcal{V}}(h)$ into the same space. In addition, we will denote by $\|\cdot\|_{\mathcal{L}(\boldsymbol{\mathcal{V}}_h,\boldsymbol{\mathcal{V}}(h))}$ the norm of an operator restricted to the discrete subspace $\boldsymbol{\mathcal{V}}_h$; namely, if $\boldsymbol{L} : \boldsymbol{\mathcal{V}}(h) \to \boldsymbol{\mathcal{V}}(h)$, then

$$\|\boldsymbol{L}\|_{\mathcal{L}(\boldsymbol{\mathcal{V}}_h,\boldsymbol{\mathcal{V}}(h))} := \sup_{\boldsymbol{0}\neq\boldsymbol{\tau}_h\in\boldsymbol{\mathcal{V}}_h} \frac{\|\boldsymbol{L}\boldsymbol{\tau}_h\|_{\boldsymbol{\mathcal{V}}(h)}}{\|\boldsymbol{\tau}_h\|_{\boldsymbol{\mathcal{V}}(h)}}.$$

Our first task is to prove the following properties:

- P1. $\|\boldsymbol{T} - \boldsymbol{T}_h\|_{\mathcal{L}(\boldsymbol{\mathcal{V}}_h,\boldsymbol{\mathcal{V}}(h))} \to 0$ as $h \to 0$.
- P2. $\forall \boldsymbol{\tau} \in \boldsymbol{\mathcal{V}}$, there holds

$$\inf_{\boldsymbol{\tau}_h\in\boldsymbol{\mathcal{V}}_h} \|\boldsymbol{\tau} - \boldsymbol{\tau}_h\|_{\boldsymbol{\mathcal{V}}(h)} \to 0 \quad \text{as} \quad h \to 0.$$

We need this properties in order to establish spectral correctness (see [6]) for all the discrete methods (symmetric or nonsymmetric). Property P2 is immediate as a consequence of the density of continuous piecewise degree k polynomial functions in $\boldsymbol{\mathcal{V}}$. On the other hand, P1 is not direct, and our goal is to prove it.

The following convergence result holds for the continuous and discrete solution operators.

Lemma 2 *For all $\boldsymbol{f} \in \boldsymbol{\mathcal{V}}$, the following estimate holds*

$$\|(\boldsymbol{T} - \boldsymbol{T}_h)\boldsymbol{f}\|_{\boldsymbol{\mathcal{V}}(h)} \lesssim h^s \|\boldsymbol{f}\|_{0,\Omega},$$

where $s > 0$ and the hidden constant is independent of h.

Proof From the definition of the continuous and discrete solutions operators, we have $\widehat{\boldsymbol{u}} := \boldsymbol{T}\boldsymbol{f}$ and $\widehat{\boldsymbol{u}}_h := \boldsymbol{T}_h\boldsymbol{f}$. Now, since $\widehat{\boldsymbol{u}}_h$ is the DG approximation of the velocity $\widehat{\boldsymbol{u}}$, then $\|\widehat{\boldsymbol{u}} - \widehat{\boldsymbol{u}}_h\|_{\mathcal{V}(h)}$ is precisely the error of the DG method applied on the source problem. Hence, the following Céa estimate holds

$$\begin{aligned}\|(\boldsymbol{T} - \boldsymbol{T}_h)\boldsymbol{f}\|_{\boldsymbol{\mathcal{V}}(h)} &\leq \|(\widehat{\boldsymbol{u}} - \widehat{\boldsymbol{u}}_h, \widehat{p} - \widehat{p}_h)\|_{\boldsymbol{\mathcal{V}}(h)\times\mathcal{Q}_h} \\ &\lesssim \left(1 + \frac{M_{DG}}{\beta}\right) \inf_{(\widehat{\boldsymbol{v}}_h,\widehat{q}_h)\in\boldsymbol{\mathcal{V}}_h\times\mathcal{Q}_h} \|(\widehat{\boldsymbol{u}}, \widehat{p}) - (\widehat{\boldsymbol{v}}_h, \widehat{q}_h)\|_{\boldsymbol{\mathcal{V}}(h)\times\mathcal{Q}_h},\end{aligned}$$

where the pair $(\widehat{\boldsymbol{u}}, \widehat{p}_h) \in \boldsymbol{\mathcal{V}}_h \times \mathcal{Q}_h$ is precisely the solution of the discrete source problem (7) and the hidden constant is independent of h. Now, If $\Pi_h\widehat{\boldsymbol{u}}$ represents the Lagrange interpolation of $\widehat{u}_h$ (see for instance [9]), there holds

$$\|\widehat{\boldsymbol{u}} - \widehat{\boldsymbol{u}}_h\|_{\mathcal{V}(h)} \lesssim \|\widehat{\boldsymbol{u}} - \Pi_h\widehat{\boldsymbol{u}}\|_{\mathcal{V}(h)} = \|\widehat{\boldsymbol{u}} - \Pi_h\widehat{\boldsymbol{u}}\|_{1,\Omega} \leq h^s \|\widehat{\boldsymbol{u}}_h\|_{1+s} \lesssim h^s \|\boldsymbol{f}\|_{0,\Omega},$$

where we have used the additional regularity of the Stokes source problem, the approximation properties of the Lagrange operator and Remark 1. On the other hand, if $S_h : \mathcal{Q} \to \mathcal{Q}_h$ denotes the classic L^2-orthogonal projection, we have

$$\|\widehat{p} - \widehat{p}_h\|_{0,\Omega} \lesssim \|\widehat{p} - S_h\widehat{p}_h\|_{0,\Omega} \lesssim h^s \|\boldsymbol{f}\|_{0,\Omega},$$

where once again we have used Remark 1. This allows us to conclude the proof.

□

Now, we prove the analogous of the previous lemma, but considering discrete sources.

Corollary 1 *For all $\boldsymbol{f}_h \in \boldsymbol{\mathcal{V}}_h$, the following estimate holds*

$$\|(\boldsymbol{T} - \boldsymbol{T}_h)\boldsymbol{f}_h\|_{\boldsymbol{\mathcal{V}}(h)} \lesssim h^s \|\boldsymbol{f}_h\|_{\boldsymbol{\mathcal{V}}(h)},$$

where s is as in Theorem 1 and the hidden constant is independent of h.

Proof Let $\boldsymbol{f}_h \in \boldsymbol{\mathcal{V}}_h$. Invoking the previous Lemma, we conclude the proof. □

Now, we are in position to establish P1.

Lemma 3 *Therefore, following estimate holds*

$$\|\boldsymbol{T} - \boldsymbol{T}_h\|_{\mathcal{L}(\boldsymbol{\mathcal{V}}_h, \boldsymbol{\mathcal{V}}(h))} \lesssim h^s,$$

where the hidden constant is independent of h.

Proof Given $\boldsymbol{f}_h \in \boldsymbol{\mathcal{V}}_h$, we have

$$\|\boldsymbol{T} - \boldsymbol{T}_h\|_{\mathcal{L}(\boldsymbol{\mathcal{V}}_h, \boldsymbol{\mathcal{V}}(h))} := \sup_{\boldsymbol{0} \neq \boldsymbol{f}_h \in \boldsymbol{\mathcal{V}}_h} \frac{\|(\boldsymbol{T} - \boldsymbol{T}_h)\boldsymbol{f}_h\|_{\boldsymbol{\mathcal{V}}(h)}}{\|\boldsymbol{f}_h\|_{\boldsymbol{\mathcal{V}}(h)}} \lesssim h^s,$$

where we have used Lemma 1. This concludes the proof. □

From now on, $\mathcal{D}$ denotes the unitary disk defined in the complex plane by $\mathcal{D} := \{z \in \mathbb{C} : |z| \leq 1\}$. The following result proves that the continuous resolvent is bounded in the $\boldsymbol{\mathcal{V}}(h)$ norm.

Lemma 4 *There exists a constant $C > 0$ independent of h such that for all $z \in \mathcal{D} \setminus \mathrm{sp}(\boldsymbol{T})$ there holds*

$$\|(z\boldsymbol{I} - \boldsymbol{T})\boldsymbol{f}\|_{\boldsymbol{\mathcal{V}}(h)} \geq C|z| \, \|\boldsymbol{f}\|_{\boldsymbol{\mathcal{V}}(h)} \quad \forall \boldsymbol{f} \in \boldsymbol{\mathcal{V}}(h).$$

Proof For $\boldsymbol{f} \in \boldsymbol{\mathcal{V}}(h)$, we introduce

$$\boldsymbol{u}^* := \boldsymbol{T}\boldsymbol{f} \in \boldsymbol{\mathcal{V}}$$

and notice that

$$(z\boldsymbol{I}-\boldsymbol{T})\boldsymbol{u}^*=\boldsymbol{T}(z\boldsymbol{I}-\boldsymbol{T})\boldsymbol{f}.$$

Since $\boldsymbol{T}:\boldsymbol{\mathcal{V}}\to\boldsymbol{\mathcal{V}}$ is a bounded operator and using the fact that $\|(z\boldsymbol{I}-\boldsymbol{T})\,\boldsymbol{u}\|_{1,\Omega}\geq C\|\boldsymbol{u}\|_{1,\Omega}$ for $z\notin \mathrm{sp}(\boldsymbol{T})$ (see [16, Proposition 2.5] for instance), we have that

$$\begin{aligned}C\|\boldsymbol{u}^*\|_{1,\Omega}&\leq\|(z\boldsymbol{I}-\boldsymbol{T})\boldsymbol{u}^*\|_{1,\Omega}\\&=\|\boldsymbol{T}(z\boldsymbol{I}-\boldsymbol{T})\boldsymbol{f}\|_{1,\Omega}\leq\|\boldsymbol{T}\|_{\mathcal{L}(\boldsymbol{\mathcal{V}},\boldsymbol{\mathcal{V}})}\|(z\boldsymbol{I}-\boldsymbol{T})\boldsymbol{f}\|_{\boldsymbol{\mathcal{V}}(h)}.\end{aligned}$$

On the other hand, we have

$$\begin{aligned}\|\boldsymbol{f}\|_{\boldsymbol{\mathcal{V}}(h)}&\leq|z|^{-1}\|\boldsymbol{u}^*\|_{1,\Omega}+|z|^{-1}\|(z\boldsymbol{I}-\boldsymbol{T})\boldsymbol{f}\|_{\boldsymbol{\mathcal{V}}(h)}\\&\lesssim|z|^{-1}\left(1+\|\boldsymbol{T}\|_{\mathcal{L}(\boldsymbol{\mathcal{V}},\boldsymbol{\mathcal{V}})}\right)\|(z\boldsymbol{I}-\boldsymbol{T})\boldsymbol{f}\|_{\boldsymbol{\mathcal{V}}(h)}\\&\lesssim|z|^{-1}\|(z\boldsymbol{I}-\boldsymbol{T})\boldsymbol{f}\|_{\boldsymbol{\mathcal{V}}(h)}.\end{aligned}$$

Hence, $C|z|\|\boldsymbol{f}\|_{\boldsymbol{\mathcal{V}}(h)}\leq\|(z\boldsymbol{I}-\boldsymbol{T})\boldsymbol{f}\|_{\boldsymbol{\mathcal{V}}(h)}$. This concludes the proof. □

Remark 2 *Lemma 4 implies that the resolvent of $\boldsymbol{T}$ is bounded. In other words, if J is a compact subset of $\mathcal{D}\setminus\mathrm{sp}(\boldsymbol{T})$, then there exists a positive constant C independent of h, satisfying the estimate*

$$\|(z\boldsymbol{I}-\boldsymbol{T})^{-1}\|_{\mathcal{L}(\boldsymbol{\mathcal{V}}(h),\boldsymbol{\mathcal{V}}(h))}\leq C\qquad\forall z\in J.$$

Our next goal is to derive the boundedness of the discrete resolvent, when h is small enough.

Lemma 5 *If $z\in\mathcal{D}\setminus\mathrm{sp}(\boldsymbol{T})$, there exists $h_0>0$ such that for all $h\leq h_0$,*

$$\|(z\boldsymbol{I}-\boldsymbol{T}_h)\boldsymbol{f}\|_{\boldsymbol{\mathcal{V}}(h)}\geq C\,\|\boldsymbol{f}\|_{\boldsymbol{\mathcal{V}}(h)}\quad\forall\boldsymbol{f}\in\boldsymbol{\mathcal{V}}(h),$$

with $C>0$ independent of h but depending on $|z|$.

Proof The proof follows the same arguments of those in [1, Theorem 4.4], where the following triangle inequality is needed

$$\|(z\boldsymbol{I}-\boldsymbol{T}_h)\boldsymbol{f}\|_{\boldsymbol{\mathcal{V}}(h)}\geq\|(z\boldsymbol{I}-\boldsymbol{T})\boldsymbol{f}\|_{\boldsymbol{\mathcal{V}}(h)}-\|(\boldsymbol{T}-\boldsymbol{T}_h)\boldsymbol{f}\|_{\boldsymbol{\mathcal{V}}(h)},$$

together with Lemma 2 and (5). The proof is concluded tending h to zero. □

The previous lemma states that if we consider a compact subset E of the complex plane such that $E\cap\mathrm{sp}(\boldsymbol{T})=\emptyset$ for h small enough and for all $z\in E$, operator $z\boldsymbol{I}-\boldsymbol{T}_h$ is invertible. Moreover, there exists a positive constant C independent of h such that $\|(z\boldsymbol{I}-\boldsymbol{T}_h)^{-1}\|_{\mathcal{L}(\boldsymbol{\mathcal{V}}(h),\boldsymbol{\mathcal{V}}(h))}\leq C$ for all $z\in E$. This fact is important since it determines that the numerical method is spurious free for h small enough. This is summarized in the following result proved in [6].

Theorem 2 *Let $E \subset \mathbb{C}$ be a compact subset not intersecting* $\mathrm{sp}(\boldsymbol{T})$. *Then, there exists $h_0 > 0$ such that, if $h \leq h_0$, then $E \cap \mathrm{sp}(\boldsymbol{T}_h) = \emptyset$.*

We recall the definition of the resolvent operator of $\boldsymbol{T}$ and $\boldsymbol{T}_h$ respectively:

$$(z\boldsymbol{I} - \boldsymbol{T})^{-1} : \boldsymbol{\mathcal{V}} \to \boldsymbol{\mathcal{V}}, \quad z \in \mathbb{C} \setminus \mathrm{sp}(\boldsymbol{T}),$$
$$(z\boldsymbol{I} - \boldsymbol{T}_h)^{-1} : \boldsymbol{\mathcal{V}}_h \to \boldsymbol{\mathcal{V}}_h, \quad z \in \mathbb{C} \setminus \mathrm{sp}(\boldsymbol{T}_h).$$

We introduce the definition of the *gap* $\widehat{\delta}$ between two closed subspaces $\mathcal{X}$ and $\mathcal{Y}$ of $L^2(\Omega)$:

$$\widehat{\delta}(\mathcal{X}, \mathcal{Y}) := \max\left\{\delta(\mathcal{X}, \mathcal{Y}), \delta(\mathcal{Y}, \mathcal{X})\right\},$$

where

$$\delta(\mathcal{X}, \mathcal{Y}) := \sup_{x \in \mathcal{X}:\ \|x\|_{0,\Omega}=1} \left(\inf_{y \in \mathcal{Y}} \|x - y\|_{0,\Omega}\right).$$

Let λ be an isolated eigenvalue of $\boldsymbol{T}$ and let D be an open disk in the complex plane with boundary γ such that λ is the only eigenvalue of $\boldsymbol{T}$ lying in D and $\gamma \cap \mathrm{sp}(\boldsymbol{T}) = \emptyset$. We introduce the spectral projector corresponding to the continuous and discrete solution operators $\boldsymbol{T}$ and $\boldsymbol{T}_h$, respectively

$$\boldsymbol{\mathcal{E}} := \frac{1}{2\pi i} \int_\gamma (z\boldsymbol{I} - \boldsymbol{T})^{-1}\, dz : \boldsymbol{\mathcal{V}}(h) \longrightarrow \boldsymbol{\mathcal{V}}(h),$$

$$\boldsymbol{\mathcal{E}}_h := \frac{1}{2\pi i} \int_\gamma (z\boldsymbol{I} - \boldsymbol{T}_h)^{-1}\, dz : \boldsymbol{\mathcal{V}}(h) \longrightarrow \boldsymbol{\mathcal{V}}(h).$$

The following approximation result for the spectral projections holds.

Lemma 6 *There holds*

$$\lim_{h \to 0} \|\boldsymbol{\mathcal{E}} - \boldsymbol{\mathcal{E}}_h\|_{\mathcal{L}(\boldsymbol{\mathcal{V}}_h, \boldsymbol{\mathcal{V}}(h))} = 0.$$

Proof See [[1]Theorem 5.1]. □

Now, we provide an error estimate for the eigenfunctions.

Lemma 7 *For h small enough, it holds*

$$\widehat{\delta}_h(\boldsymbol{\mathcal{E}}(\boldsymbol{\mathcal{V}}), \boldsymbol{\mathcal{E}}_h(\boldsymbol{\mathcal{V}}_h)) \lesssim h^{\min\{r,k\}},$$

where the hidden constant is independent of h.

Proof To obtain this result, in virtue of the definition of $\widehat{\delta}$, we need to control the quantities $\delta_h(\boldsymbol{\mathcal{E}}(\boldsymbol{\mathcal{V}}), \boldsymbol{\mathcal{E}}_h(\boldsymbol{\mathcal{V}}_h))$ and $\delta_h(\boldsymbol{\mathcal{E}}_h(\boldsymbol{\mathcal{V}}_h), \boldsymbol{\mathcal{E}}(\boldsymbol{\mathcal{V}}))$. Let us begin deriving an estimate for $\delta_h(\boldsymbol{\mathcal{E}}_h(\boldsymbol{\mathcal{V}}_h), \boldsymbol{\mathcal{E}}(\boldsymbol{\mathcal{V}}))$. Since the continuous solution operator is defined by $\boldsymbol{T} : \boldsymbol{\mathcal{V}} \to \boldsymbol{\mathcal{V}}$, we need to operate as in the proof of [[16] Theorem 5.1]. We notice that since $\boldsymbol{\mathcal{E}}|_{\boldsymbol{\mathcal{V}}}$ is a spectral projection in $\boldsymbol{\mathcal{V}}$ onto the eigenspace $\boldsymbol{\mathcal{E}}(\boldsymbol{\mathcal{V}})$

corresponding to the eigenvalue λ of $\boldsymbol{T}$, we have $\boldsymbol{\mathcal{E}}(\boldsymbol{\mathcal{V}}(h))) = \boldsymbol{\mathcal{E}}(\boldsymbol{\mathcal{V}})$ (see [[16] equation (41)]). On the other hand, from Lemma 6, we are able to obtain the estimate $\|\boldsymbol{\mathcal{E}} - \boldsymbol{\mathcal{E}}_h\|_{\mathcal{L}(\boldsymbol{\mathcal{V}}_h, \boldsymbol{\mathcal{V}}(h))} \lesssim \|\boldsymbol{T} - \boldsymbol{T}_h\|_{\mathcal{L}(\boldsymbol{\mathcal{V}}_h, \boldsymbol{\mathcal{V}}(h))}$ (see [[16] Lemma 5.3]). Now since $\boldsymbol{\mathcal{E}}_h$ is a projector, for h sufficiently small, we have for all $\boldsymbol{v}_h \in \boldsymbol{\mathcal{E}}_h(\boldsymbol{\mathcal{V}}_h)$ the relation $\boldsymbol{\mathcal{E}}_h \boldsymbol{v}_h = \boldsymbol{v}_h$. Moreover, $\boldsymbol{\mathcal{E}} \boldsymbol{v}_h \in \boldsymbol{\mathcal{E}}(\boldsymbol{\mathcal{V}})$. Then, for all $\boldsymbol{v}_h \in \boldsymbol{\mathcal{E}}_h(\boldsymbol{\mathcal{V}}_h)$, the following estimate holds

$$\delta(\boldsymbol{v}_h, \boldsymbol{\mathcal{E}}(\boldsymbol{\mathcal{V}})) \lesssim \|\boldsymbol{\mathcal{E}}_h \boldsymbol{v}_h - \boldsymbol{\mathcal{E}} \boldsymbol{v}_h\|_{\boldsymbol{\mathcal{V}}(h)} \lesssim \|\boldsymbol{\mathcal{E}}_h - \boldsymbol{\mathcal{E}}\|_{\mathcal{L}(\boldsymbol{\mathcal{V}}_h, \boldsymbol{\mathcal{V}}(h))} \|\boldsymbol{v}_h\|_{\boldsymbol{\mathcal{V}}(h)},$$

implying that $\delta(\boldsymbol{\mathcal{E}}_h(\boldsymbol{\mathcal{V}}_h), \boldsymbol{\mathcal{E}}(\boldsymbol{\mathcal{V}})) \lesssim h^{\min\{r,k\}}$, where we have invoked Lemma 3 for $s = r$ and taking into account the corresponding minimum between r and the polynomial degree.

Now, our task is to estimate $\delta_h(\boldsymbol{\mathcal{E}}(\boldsymbol{\mathcal{V}}), \boldsymbol{\mathcal{E}}_h(\boldsymbol{\mathcal{V}}_h))$. It is easy to check that the IPDG methods are consistent in the sense that for all $(\boldsymbol{v}_h, q_h) \in \boldsymbol{\mathcal{V}}_h \times \mathcal{Q}_h$, the following identity holds

$$A_h((\boldsymbol{u} - \boldsymbol{u}_h, p - p_h), (\boldsymbol{v}_h, q_h)) = 0,$$

with $(\boldsymbol{u}, p) \in [H^{1+r}(\Omega)]^d \times H^r(\Omega)$ and $r > 0$. This consistency, together with standard arguments of mixed finite element theory, leads us to the following Céa estimate

$$\|(\boldsymbol{u} - \boldsymbol{u}_h, p - p_h)\|_{\boldsymbol{\mathcal{V}}(h) \times \mathcal{Q}_h} \lesssim \left(1 + \frac{M_{DG}}{\beta}\right) \inf_{(\boldsymbol{v}_h, q_h) \in \boldsymbol{\mathcal{V}}_h \times \mathcal{Q}_h} \|(\boldsymbol{u}, p) - (\boldsymbol{v}_h, q_h)\|_{\boldsymbol{\mathcal{V}}(h) \times \mathcal{Q}_h},$$

where M_{DG} and β are the continuity constant of $a_h(\cdot, \cdot)$ and the inf-sup constant of $b_h(\cdot, \cdot)$, respectively. Now, from the properties of the Lagrange interpolation operator (see [9] for instance) and the L^2 orthogonal projection operator, together with the additional regularity provided by the invariant space $\boldsymbol{\mathcal{E}}(\boldsymbol{\mathcal{V}})$, which in our case is $\boldsymbol{u} \in \boldsymbol{\mathcal{E}}(\boldsymbol{\mathcal{V}}) \subset [H^{1+r}(\Omega)]^d$ with $r > 0$, we have

$$\|(\boldsymbol{u} - \boldsymbol{u}_h, p - p_h)\|_{\boldsymbol{\mathcal{V}}(h) \times \mathcal{Q}_h} \lesssim h^{\min\{r,k\}} (\|\boldsymbol{u}\|_{1+r} + \|p\|_{r,\Omega}).$$

This allows us to conclude the proof. □

The next result provides, for the proposed IPDG methods, a double order of convergence for the eigenvalues. More precisely, the result presents estimates for symmetric and nonsymmetric methods, where optimal and suboptimal order of convergence are attained, respectively.

Theorem 3 *There exists a strictly positive constant h_0 such that, for $h < h_0$, there holds*

(1) If the symmetric IPDG method is considered ($\varepsilon = 1$), then there holds

$$|\lambda - \lambda_h| \lesssim h^{2\min\{r,k\}}, \tag{10}$$

(2) If any of the nonsymmetric IPDG methods are considered ($\varepsilon \in \{-1, 0\}$), then there holds

$$|\lambda - \lambda_h| \lesssim h^{\min\{r,k\}}, \tag{11}$$

where in each estimate, the hidden constant is independent of h.

Proof Observe that (11) is a direct consequence of Lemma 7. Now, to prove (10), let us consider the following well-known algebraic identity:

$$A_h((\boldsymbol{u}-\boldsymbol{u}_h,\, p-p_h),(\boldsymbol{u}-\boldsymbol{u}_h,\, p-p_h))-\lambda(\boldsymbol{u}-\boldsymbol{u}_h,\boldsymbol{u}-\boldsymbol{u}_h)=\left(\lambda_{i,h}-\lambda\right)(\boldsymbol{u}_h,\boldsymbol{u}_h).$$

On the other hand, invoking (9), we have

$$(\boldsymbol{u}_h,\boldsymbol{u}_h)=\frac{A_h((\boldsymbol{u}-\boldsymbol{u}_h,\, p-p_h),(\boldsymbol{u}-\boldsymbol{u}_h,\, p-p_h))}{|\lambda_{i,h}|}\geq\frac{\alpha\|\boldsymbol{u}_h\|^2_{\boldsymbol{\mathcal{V}}(h)}}{|\lambda_{i,h}|}\geq\widehat{C}>0.$$

Since $A_h(\cdot,\cdot)$ is a bounded bilinear form, we have

$$\widehat{C}|\lambda_{i,h}-\lambda|\leq|A_h((\boldsymbol{u}-\boldsymbol{u}_h,\, p-p_h),(\boldsymbol{u}-\boldsymbol{u}_h,\, p-p_h))|+|\lambda||(\boldsymbol{u}-\boldsymbol{u}_h,\boldsymbol{u}-\boldsymbol{u}_h)|. \quad (12)$$

For the first term on the right hand side of (12), we have

$$|A_h((\boldsymbol{u}-\boldsymbol{u}_h,\, p-p_h),(\boldsymbol{u}-\boldsymbol{u}_h,\, p-p_h))|=|a_h(\boldsymbol{u}-\boldsymbol{u}_h,\boldsymbol{u}-\boldsymbol{u}_h)|\leq\|\boldsymbol{u}-\boldsymbol{u}_h\|^2_{\boldsymbol{\mathcal{V}}(h)}.$$

Then, since $\boldsymbol{u}\in\boldsymbol{\mathcal{E}}(\boldsymbol{\mathcal{V}})$, we have

$$\|\boldsymbol{u}_h-\boldsymbol{u}\|_{\boldsymbol{\mathcal{V}}(h)}=\delta(\boldsymbol{u}_h,\boldsymbol{\mathcal{E}}(\boldsymbol{\mathcal{V}}))\lesssim\widehat{\delta}(\boldsymbol{\mathcal{E}}_h(\boldsymbol{\mathcal{V}}_h),\boldsymbol{\mathcal{E}}(\boldsymbol{\mathcal{V}}_h))\lesssim h^{\min\{r,k\}}. \quad (13)$$

On the other hand,

$$\|\boldsymbol{u}-\boldsymbol{u}_h\|_{0,\Omega}\lesssim\|\boldsymbol{u}-\boldsymbol{u}_h\|_{\boldsymbol{\mathcal{V}}(h)}\lesssim h^{\min\{r,k\}}, \quad (14)$$

where we have used the Poincaré inequality (5) and the same arguments that derive (13). Hence, gathering (13), (14) and replacing these estimates in (12), we conclude the proof. □

5 Numerical experiments

In this section, we report some numerical tests in order to assess the performance of the proposed numerical method, in the computation of the eigenvalues of problem (7).

We report numerical results for the three different DG discretizations to solve the Stokes eigenvalue problem, namely, for $\varepsilon\in\{-1,0,1\}$. These results have been obtained using a FEniCS code [15], and the considered meshes are the ones provided by this software. We will present two different situations: The first consists of applying the method to solve the Stokes eigenvalue problem considering mixed boundary conditions

in order to observe if the method introduce spurious eigenvalues. In particular, we will analyze the influence stabilization parameter $\mathtt{a}_S$. We note that other spectral analysis using DG methods introduce spurious eigenvalues when the stabilization parameter is not correctly chosen (see, for instance, [16, 17]). Hence, our intention in this test is to identify a safe threshold in which we can compute the spectrum correctly.

On the other hand, in the second test, we apply the method considering homogeneous Dirichlet conditions in order to approximate smooth eigenfunctions and obtain rates of convergence. These two scenarios will be tested for the SIP ($\varepsilon = 1$), NIP ($\varepsilon = -1$), and IIP ($\varepsilon = 0$) methods in order to compare them.

From now on, the stabilization parameter $\mathtt{a}_S$ in the bilinear form $a_h(\cdot,\cdot)$ (cf. (8)) will be chosen proportionally to the square of the polynomial degree k as $\mathtt{a}_S = \mathtt{a}k^2$ with $\mathtt{a} > 0$. For simplicity, we have taken $\nu = 1$ as kinematic viscosity.

5.1 Square with mixed boundary conditions

In the forthcoming experiments, we are only concerned in the effects of the stabilization parameter on the computation of the spectrum. For this test, the computational domain is the unitary square $\Omega = (0,1)^2$. The boundary conditions are $\boldsymbol{u} = \mathbf{0}$ on the bottom of the square, and, on the rest, we assume that the sides of the square are free of stress, namely, $(\nabla \boldsymbol{u} - p\mathbb{I}) \cdot \boldsymbol{n} = \mathbf{0}$. Due the geometrical and physical configuration of this domain, it is expectable that spurious eigenvalues arise when the stabilization parameter is not chosen properly. This motivates the study of the effects of the stabilization parameter on the computation of the spectrum.

In Fig. 1, we present an example of the meshes for our experiments. We remark that these meshes are provided by FEniCS. For other domains, we also consider the meshes of FEniCS.

Since in this test we are considering mixed boundary conditions, spurious eigenvalues are expected for certain stabilization parameters, as, for example, in [16] and [17] for the elasticity and Stokes spectral problems, respectively, where this phenomenon is also observed. To make matters precise, the forthcoming results show the effects in

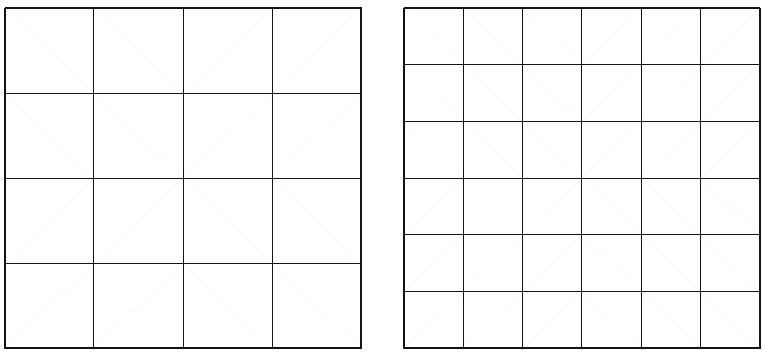

Fig. 1 Examples of the meshes used in the unit square. The left figure represents a mesh for $N = 4$ and the right one for $N = 6$

Table 1 Computed eigenvalues for $k = 2$, refinement level of the mesh $N = 8$, and different stabilization values

$\mathtt{a} = 1/4$	$\mathtt{a} = 1/2$	$\mathtt{a} = 1$	$\mathtt{a} = 2$	$\mathtt{a} = 4$	$\mathtt{a} = 8$
−51.5827843	−38.0086353	−25.7741157	2.4673967	2.4673984	2.4673995
2.4673994	2.4674060	−7.7428930	6.2823213	6.2837898	6.2846799
6.2807623	6.2836221	2.4673951	15.2191850	15.2250578	15.2289821
15.2197528	15.2247397	4.0187272	22.2069897	22.2082373	22.2089953
22.2090093	22.2304253	6.4215943	26.9585220	26.9655945	26.9702116
26.9419996	26.9500426	15.3198683	43.1596990	43.1813564	43.1958316
32.6879700	31.3711601	22.2040077	48.4095301	48.4608496	48.4962729
43.2234986	43.0886035	23.4674407	61.6948903	61.7207719	61.7360376
48.4030389	48.5151481	27.1142786	64.3707811	64.4286742	64.4646562
61.7382092	61.6745849	32.5589528	75.3545722	75.5091440	75.6186050

the choice of $\mathtt{a}$ when the SIP, NIP, and IIP methods are considered for the computation of the spectrum.

5.1.1 SIP method

In this test, we set $\varepsilon = 1$ in (8). To observe the behavior of the spurious eigenvalues respect to the stabilization parameter, the strategy here consists into fix a refinement parameter N and compute the spectrum for different values of $\mathtt{a}$. We begin with the computation of eigenvalues with different stabilizations and polynomial degrees, fixing the refinement level on $N = 8$.

Table 2 Computed eigenvalues for $k = 3$, refinement level of the mesh $N = 8$, and different stabilization values

$\mathtt{a} = 1/4$	$\mathtt{a} = 1/2$	$\mathtt{a} = 1$	$\mathtt{a} = 2$	$\mathtt{a} = 4$	$\mathtt{a} = 8$
−25.8911566	2.4673962	2.4673962	2.4673962	2.4673962	2.4673962
−6.9533161	6.2800172	6.2807543	6.2798261	6.2799516	6.2800197
1.3671713	15.2113035	15.2137332	15.2106882	15.2110819	15.2112975
2.4673962	22.2065701	22.2065631	22.2065701	22.2065714	22.2065723
6.2802957	26.9499653	26.9508745	26.9495553	26.9498729	26.9500458
15.2108124	43.1443102	43.1471293	43.1436341	43.1442823	43.1446839
22.2065688	48.3474162	48.3562431	48.3440788	48.3465144	48.3478748
26.9362671	61.6852113	61.6847819	61.6851692	61.6852465	61.6853014
27.6605592	64.3094958	64.3180603	64.3072318	64.3091509	64.3102899
28.3620195	75.2194409	75.2351965	75.2149097	75.2200868	75.2234502

Table 3 Computed eigenvalues for $k = 4$, refinement level of the mesh $N = 8$, and different stabilization values

$\mathtt{a} = 1/4$	$\mathtt{a} = 1/2$	$\mathtt{a} = 1$	$\mathtt{a} = 2$	$\mathtt{a} = 4$	$\mathtt{a} = 8$
−23.7579288	2.4673962	2.4673962	2.4673962	2.4673962	2.4673962
−12.6239007	6.2795001	6.2794428	6.2795049	6.2795263	6.2795376
2.4673962	15.2096059	7.3180634	15.2096921	15.2097587	15.2097936
6.2794847	22.2065655	15.2098219	22.2065655	22.2065655	22.2065655
15.2095018	26.9487029	22.2065655	26.9487045	26.9487594	26.9487890
22.2065655	43.1420482	22.7715111	43.1420939	43.1421826	43.1422299
26.0942752	48.3368059	26.9492760	48.3377321	48.3381475	48.3383709
26.9485754	61.6849077	43.1420081	61.6849052	61.6849056	61.6849059
43.1418083	64.3021502	48.3373849	64.3023792	64.3026819	64.3028435
48.3363308	75.2020647	61.6849042	75.2025415	75.2032383	75.2036188

From Tables 1, 2, 3, 4, and 5, we observe that spurious eigenvalues appear when $\mathtt{a} \leq 1$ for each polynomial degree. However, when k increases, the presence of physical eigenvalues predominates compared with the spurious ones. Moreover, this test reveals that for $\mathtt{a} > 1$, the computation of the spectrum is safe.

5.1.2 NIP method

For this test, we set $\varepsilon = -1$ in (8). Since the method is nonsymmetric, the matrix associated with $A_h(\cdot, \cdot)$, in general, is nonsymmetric as well. This fact leads to the presence of complex eigenvalues in the computed spectrum. In order to present the tables, we only report the real part of the computed eigenvalues.

Table 4 Computed eigenvalues for $k = 5$, refinement level of the mesh $N = 8$, and different stabilization values

$\mathtt{a} = 1/4$	$\mathtt{a} = 1/2$	$\mathtt{a} = 1$	$\mathtt{a} = 2$	$\mathtt{a} = 4$	$\mathtt{a} = 8$
−39.1823755	−45.6379054	−18.0818408	2.4673962	2.4673962	2.4673962
−3.6023959	2.4673962	2.4673962	6.2794043	6.2794091	6.2794108
2.4673962	6.2793257	6.2794179	15.2093787	15.2093935	15.2093991
6.2794411	15.2093065	15.2094129	22.2065655	22.2065655	22.2065655
15.2096639	22.2065655	22.2065655	26.9484479	26.9484594	26.9484637
22.2065654	26.9481586	26.9484956	43.1416731	43.1416927	43.1417001
26.9484204	43.1411160	43.1417131	48.3357858	48.3358742	48.3359077
43.1417325	48.3349732	48.3360290	61.6849041	61.6849041	61.6849042
48.3353715	61.6849040	61.6849041	64.3009605	64.3010269	64.3010520
61.6849040	64.2985669	64.3010532	75.1992565	75.1994045	75.1994604

Table 5 Computed eigenvalues for $k = 6$, refinement level of the mesh $N = 8$, and different stabilization values

$\mathtt{a} = 1/4$	$\mathtt{a} = 1/2$	$\mathtt{a} = 1$	$\mathtt{a} = 2$	$\mathtt{a} = 4$	$\mathtt{a} = 8$
−17.7169206	2.4673962	−11.5796563	2.4673962	2.4673962	2.4673962
2.4673962	6.2793877	2.4673962	6.2793742	6.2793757	6.2793763
6.2793838	11.9560755	6.2793735	15.2092840	15.2092888	15.2092906
15.2093235	15.2096875	15.2092769	22.2065655	22.2065654	22.2065655
22.2065654	22.2065654	22.2065654	26.9483737	26.9483774	26.9483788
26.9483773	26.9483999	26.9483632	43.1415472	43.1415535	43.1415559
43.1415741	43.1415828	43.1415383	48.3352156	48.3352437	48.3352544
48.3355123	48.3356899	48.3351890	61.6849040	61.6849041	61.6849043
61.6849040	61.6849040	61.6849040	64.3005376	64.3005590	64.3005673
64.2995331	64.3005816	64.3004917	75.1983010	75.1983484	75.1983665

Once again, we fix the refinement level of the mesh on $N = 8$ and consider different polynomial degrees.

We observe that for the NIP method for any stabilization that we choose and any polynomial degree, there is no spurious eigenvalues when we compute the spectrum. This is a better result compared with the SIP method. For the IIP, the results are similar. Hence, we do not incorporate since the conclusion is the same as for the NIP method.

To end this section, we present in Fig. 2 plots of the velocity field associated with the first three eigenfunctions of the unitary square with mixed boundary conditions, whereas in Fig. 3, the plots represent the pressure fluctuation on this setting. The plots have been obtained with $\mathtt{a} = 10$, $N = 20$ and $k = 2$ considering the NIP method. We remark that when the SIP and IIP methods are considered, and for $\mathtt{a} > 10$ and $k > 1$, in general, the plots are similar (Tables 6, 7, 8, 9, 10).

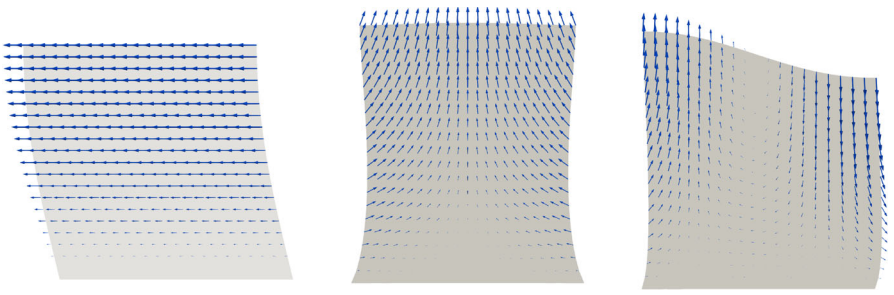

Fig. 2 Velocity fields associated with the first, second, and third eigenfunctions. These plots have been obtained with $\mathtt{a} = 10$, $N = 20$, and $k = 2$ for the NIP method

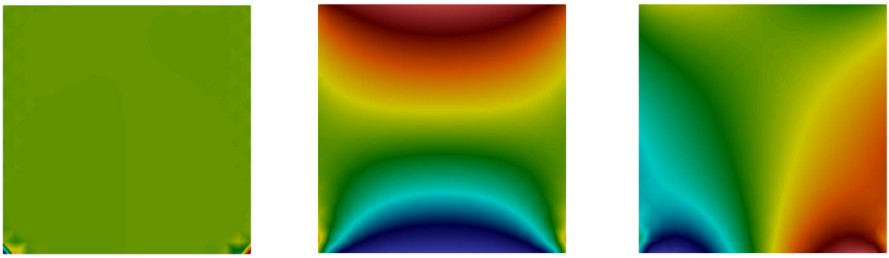

Fig. 3 Pressure fluctuation associated with the first, second, and third eigenfunctions. These plots have been obtained with $\mathtt{a} = 10$, $N = 20$, and $k = 2$ for the NIP method

Table 6 Computed eigenvalues for $k = 2$, refinement level of the mesh $N = 8$, and different stabilization values

$\mathtt{a} = 1/16$	$\mathtt{a} = 1/8$	$\mathtt{a} = 1/4$	$\mathtt{a} = 1/2$	$\mathtt{a} = 1$	$\mathtt{a} = 2$
2.4699176	2.4697962	2.4695950	2.4692963	2.4689102	2.4684867
6.2857132	6.2857494	6.2858166	6.2859957	6.2864213	6.2870959
15.2996858	15.2972945	15.2931330	15.2867796	15.2786188	15.2698076
22.4079792	22.3983103	22.3822392	22.3583846	22.3276595	22.2941663
27.1879249	27.1759397	27.1563688	27.1288184	27.0967965	27.0661281
43.9493286	43.9158153	43.8592391	43.7743383	43.6648958	43.5461418
49.2058990	49.1621884	49.0933412	49.0005606	48.8981248	48.8059789
63.2071642	63.1346623	63.0137592	62.8346721	62.6059930	62.3598511
65.7218704	65.6571088	65.5490650	65.3926356	65.2039891	65.0159306
77.3486064	77.2689570	77.1369295	76.9457888	76.7150977	76.4854844

Table 7 Computed eigenvalues for $k = 3$, refinement level of the mesh $N = 8$, and different stabilization values

$\mathtt{a} = 1/16$	$\mathtt{a} = 1/8$	$\mathtt{a} = 1/4$	$\mathtt{a} = 1/2$	$\mathtt{a} = 1$	$\mathtt{a} = 2$
2.4674078	2.4674077	2.4674075	2.4674073	2.4674070	2.4674067
6.2802294	6.2801095	6.2799319	6.2797152	6.2795241	6.2794457
15.2101531	15.2100221	15.2098849	15.2098225	15.2099299	15.2102326
22.2079387	22.2078653	22.2077461	22.2075775	22.2073748	22.2071695
26.9528604	26.9523855	26.9517237	26.9509595	26.9502662	26.9498301
43.1519319	43.1512400	43.1503727	43.1495236	43.1488604	43.1483415
48.3513208	48.3498997	48.3482557	48.3469812	48.3466700	48.3473697
61.7123006	61.7107512	61.7082435	61.7047107	61.7004727	61.6961768
64.3417568	64.3373979	64.3315462	64.3251209	64.3194410	64.3154425
75.2569989	75.2525652	75.2478248	75.2446788	75.2442038	75.2451066

Table 8 Computed eigenvalues for $k = 4$, refinement level of the mesh $N = 8$, and different stabilization values

$a = 1/16$	$a = 1/8$	$a = 1/4$	$a = 1/2$	$a = 1$	$a = 2$
2.4674058	2.4674059	2.4674059	2.4674059	2.4674059	2.4674060
6.2795865	6.2795814	6.2795767	6.2795729	6.2795675	6.2795596
15.2102536	15.2102239	15.2101749	15.2101004	15.2100044	15.2099099
22.2065207	22.2065286	22.2065413	22.2065597	22.2065824	22.2066054
26.9488997	26.9488918	26.9488882	26.9488909	26.9488921	26.9488839
43.1422553	43.1422577	43.1422507	43.1422229	43.1421750	43.1421324
48.3411012	48.3409231	48.3406402	48.3402355	48.3397398	48.3392602
61.6824677	61.6826277	61.6828874	61.6832611	61.6837192	61.6841812
64.3033286	64.3032704	64.3031825	64.3030563	64.3028993	64.3027638
75.2066217	75.2064714	75.2061795	75.2056641	75.2049292	75.2041863

Table 9 Computed eigenvalues for $k = 5$, refinement level of the mesh $N = 8$, and different stabilization values

$a = 1/16$	$a = 1/8$	$a = 1/4$	$a = 1/2$	$a = 1$	$a = 2$
2.4674060	2.4674060	2.4674060	2.4674060	2.4674060	2.4674060
6.2794252	6.2794287	6.2794323	6.2794344	6.2794338	6.2794321
15.2092443	15.2092618	15.2092863	15.2093154	15.2093452	15.2093721
22.2066536	22.2066536	22.2066537	22.2066538	22.2066539	22.2066540
26.9484447	26.9484537	26.9484655	26.9484771	26.9484859	26.9484931
43.1413330	43.1413616	43.1414069	43.1414695	43.1415428	43.1416123
48.3346507	48.3347519	48.3349064	48.3351104	48.3353415	48.3355657
61.6851085	61.6851111	61.6851154	61.6851215	61.6851287	61.6851358
64.3001194	64.3002303	64.3003835	64.3005606	64.3007361	64.3008948
75.1972111	75.1973821	75.1976577	75.1980454	75.1985012	75.1989331

Table 10 Computed eigenvalues for $k = 6$, refinement level of the mesh $N = 8$, and different stabilization values

$a = 1/16$	$a = 1/8$	$a = 1/4$	$a = 1/2$	$a = 1$	$a = 2$
2.4674060	2.4674060	2.4674060	2.4674060	2.4674060	2.4674060
6.2793946	6.2793960	6.2793984	6.2794020	6.2794057	6.2794081
15.2093701	15.2093688	15.2093664	15.2093621	15.2093551	15.2093460
22.2066544	22.2066544	22.2066544	22.2066543	22.2066543	22.2066543
26.9484505	26.9484527	26.9484564	26.9484617	26.9484667	26.9484687
43.1417231	43.1417151	43.1417015	43.1416808	43.1416542	43.1416273
48.3358167	48.3358038	48.3357801	48.3357392	48.3356781	48.3356044
61.6851539	61.6851537	61.6851534	61.6851529	61.6851524	61.6851518
64.3011214	64.3011203	64.3011166	64.3011053	64.3010779	64.3010303
75.1993671	75.1993174	75.1992335	75.1991071	75.1989479	75.1987919

5.2 Rigid square

In this test, we consider as computational domain the square $\Omega := (-1, 1)^2$, and the considered meshes are like the presented in Fig. 1. We assume the condition $\boldsymbol{u} = \boldsymbol{0}$ on the whole boundary Γ. This implies that the condition $\int_\Omega p = 0$ is incorporated in the matrix system as a Lagrange multiplier. Our aim is to compare the SIP, NIP, and IIP methods, particularly on the convergence order of approximation with different polynomial degrees.

In the forthcoming tables, we present the computed eigenvalues with different meshes, the order of convergence, and extrapolate values. These values have been obtained with a least square fitting of the form $\lambda_{hi} \approx \lambda_i + C_i h^{\alpha_i}$, where $C_i \in \mathbb{R}$, for all $i \in \mathbb{N}$. This fitting has been done for each eigenvalue separately. The fitted parameters λ_i and α_i are the reported extrapolated vibration frequency λ_{extr} and estimated order of convergence, respectively.

In Tables 11, 12, and 13, we report the first six computed eigenvalues for different meshes and different methods. In Table 11, the eigenvalues have been computed with the SIP method. We observe clearly the double order of convergence. More precisely, the order of convergence is $\mathcal{O}(h^{2k})$, where k is the polynomial degree. On the

Table 11 Smallest computed eigenvalues for polynomial degrees $k = 1, 2, 3$, $\mathtt{a} = 8$, and $\varepsilon = 1$

k	$N = 10$	$N = 20$	$N = 30$	$N = 40$	Order	λ_{extr}	[20]	[19]
1	13.4868	13.1853	13.1272	13.1089	1.98	13.0823	13.0860	13.086
	24.1190	23.3116	23.1487	23.1003	1.93	23.0217	23.0308	23.031
	24.2360	23.3210	23.1566	23.1019	2.06	23.0321	23.0308	23.031
	34.4884	32.6529	32.3007	32.1922	1.99	32.0318	32.0443	32.053
	41.3628	39.3010	38.8512	38.7208	1.82	38.4778	38.5252	38.532
	44.9594	42.6074	42.1248	41.9708	1.88	41.7251	41.7588	41.759
2	13.0902	13.0865	13.0862	13.0862	3.64	13.0861	13.0860	13.086
	23.0465	23.0322	23.0312	23.0311	3.63	23.0309	23.0308	23.031
	23.0488	23.0323	23.0312	23.0311	3.68	23.0309	23.0308	23.031
	32.1109	32.0562	32.0530	32.0525	3.89	32.0522	32.0443	32.053
	38.5981	38.5358	38.5320	38.5314	3.84	38.5310	38.5252	38.532
	41.8338	41.7630	41.7582	41.7576	3.69	41.7570	41.7588	41.759
3	13.0862	13.0861	13.0861	13.0861	5.31	13.0861	13.0860	13.086
	23.0312	23.0310	23.0310	23.0310	5.26	23.0310	23.0308	23.031
	23.0312	23.0310	23.0310	23.0310	5.52	23.0310	23.0308	23.031
	32.0530	32.0523	32.0523	32.0523	5.27	32.0523	32.0443	32.053
	38.5320	38.5311	38.5312	38.5312	5.78	38.5312	38.5252	38.532
	41.7584	41.7572	41.7572	41.7572	5.44	41.7572	41.7588	41.759

Table 12 Smallest computed eigenvalues for polynomial degrees $k = 1, 2, 3$, $\mathtt{a} = 8$, and $\varepsilon = -1$

k	$N = 10$	$N = 20$	$N = 30$	$N = 40$	Order	λ_{extr}	[20]	[19]
1	13.2778	13.1302	13.1034	13.0959	2.10	13.0849	13.0860	13.086
	23.5280	23.1602	23.0847	23.0614	1.89	23.0233	23.0308	23.031
	23.6616	23.1602	23.0863	23.0614	2.35	23.0381	23.0308	23.031
	33.1704	32.3229	32.1674	32.1140	2.02	32.0454	32.0443	32.053
	39.9729	38.8834	38.6743	38.6146	2.01	38.5209	38.5252	38.532
	43.4244	42.1522	41.9255	41.8515	2.08	41.7573	41.7588	41.759
2	13.1217	13.0946	13.0896	13.0881	2.05	13.0860	13.0860	13.086
	23.1337	23.0561	23.0413	23.0370	2.02	23.0305	23.0308	23.031
	23.1411	23.0573	23.0417	23.0371	2.05	23.0304	23.0308	23.031
	32.3113	32.1066	32.0740	32.0645	2.28	32.0533	32.0443	32.053
	38.8366	38.6011	38.5597	38.5481	2.14	38.5317	38.5252	38.532
	42.0862	41.8367	41.7903	41.7765	2.05	41.7566	41.7588	41.759
3	13.0865	13.0861	13.0861	13.0861	4.44	13.0861	13.0860	13.086
	23.0324	23.0311	23.0310	23.0310	4.03	23.0310	23.0308	23.031
	23.0328	23.0311	23.0310	23.0310	4.13	23.0310	23.0308	23.031
	32.0570	32.0526	32.0523	32.0523	3.96	32.0523	32.0443	32.053
	38.5372	38.5315	38.5312	38.5312	3.95	38.5312	38.5252	38.532
	41.7649	41.7577	41.7573	41.7572	3.89	41.7572	41.7588	41.759

Table 13 Smallest computed eigenvalues for polynomial degrees $k = 1, 2, 3$, $\mathtt{a} = 8$, and $\varepsilon = 0$

k	$N = 10$	$N = 20$	$N = 30$	$N = 40$	Order	λ_{extr}	[20]	[19]
1	13.3569	13.1507	13.1121	13.1006	2.04	13.0840	13.0860	13.086
	23.7551	23.2185	23.1080	23.0759	1.91	23.0217	23.0308	23.031
	23.8801	23.2185	23.1121	23.0759	2.22	23.0378	23.0308	23.031
	33.6842	32.4475	32.2166	32.1427	2.02	32.0410	32.0443	32.053
	40.4995	39.0387	38.7391	38.6536	1.92	38.5080	38.5252	38.532
	44.0067	42.3206	41.9984	41.8950	1.98	41.7463	41.7588	41.759
2	13.1073	13.0909	13.0880	13.0872	2.15	13.0861	13.0860	13.086
	23.0943	23.0453	23.0368	23.0343	2.16	23.0310	23.0308	23.031
	23.0993	23.0460	23.0369	23.0344	2.20	23.0311	23.0308	23.031
	32.2209	32.0837	32.0645	32.0590	2.47	32.0535	32.0443	32.053
	38.7298	38.5716	38.5472	38.5406	2.34	38.5325	38.5252	38.532
	41.9738	41.8035	41.7758	41.7680	2.26	41.7583	41.7588	41.759
3	13.0864	13.0862	13.0861	13.0861	4.49	13.0861	13.0860	13.086
	23.0319	23.0310	23.0310	23.0310	4.06	23.0310	23.0308	23.031
	23.0322	23.0311	23.0310	23.0310	4.21	23.0310	23.0308	23.031
	32.0554	32.0525	32.0523	32.0523	4.04	32.0523	32.0443	32.053
	38.5352	38.5314	38.5312	38.5312	4.04	38.5312	38.5252	38.532
	41.7623	41.7575	41.7573	41.7572	3.99	41.7573	41.7588	41.759

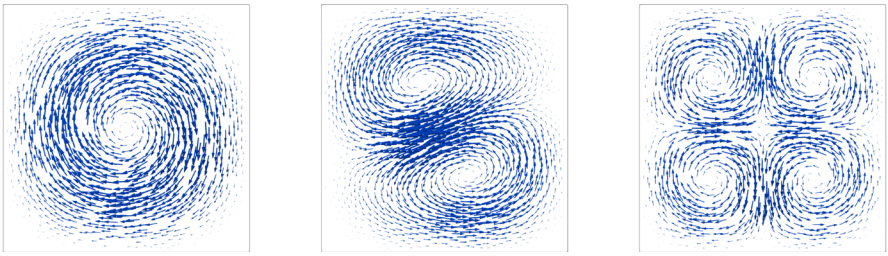

Fig. 4 Velocity fields associated with the first, second, and third eigenfunctions. These plots have been obtained with $\mathtt{a} = 8$, $N = 30$, and $k = 3$ for the NIP method

other hand, for the nonsymmetric methods, a variation on the order of convergence is observed.

To make matters precise, in both methods (for $\varepsilon \in \{-1, 0\}$), when k is even, the order of convergence is $\mathcal{O}(h^k)$, whereas when k is odd, the order is $\mathcal{O}(h^{k+1})$. These results are expectable, since when the DG method has been applied in other contexts as in [3] for Maxwell's spectral problem, the behavior on the computed order of convergence for symmetric and nonsymmetric methods is similar to our problem. Also, for the pseudostress formulation of the Stokes spectral problem analyzed in [17], the order of convergence is also the same.

An important fact on the computation of the spectrum when the nonsymmetric methods are considered is the complex eigenvalues. In some cases, these complex results arise. For example, for the NIP method ($\varepsilon = -1$), $k = 1$ and $N = 20$, the second and third eigenvalues, which are double, are in fact $\lambda_h = 23.160181519681554 \pm 0.003363156781536\, i$, where the imaginary part is small compared with the real part of the eigenvalue. For the IIP method ($\varepsilon = 0$), we have observed, for $k = 1$, a similar result, i.e, $\lambda_h = 23.218511272886694 \pm 0.001801568783833\, i$. When $k > 1$, we have not observed complex eigenvalues on the computed spectrum.

We end this test presenting plots of the velocity fields (Fig. 4) and pressure fluctuations (Fig. 5) for the rigid square domain. These plots have been obtained with the NIP method, for $\mathtt{a} = 8$, $N = 30$, and $k = 3$.

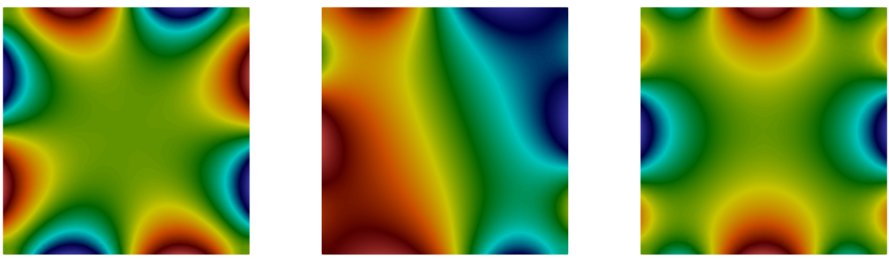

Fig. 5 Pressure fluctuation associated with the first, third, and fourth eigenfunctions. These plots have been obtained with $\mathtt{a} = 8$, $N = 30$, and $k = 3$ for the NIP method

5.3 Circular, non-convex, and three dimensional domains

In the following tests, we are only interested in the computation of convergence order for the method, for different domains. In particular, the domains under consideration are a unit circle, an L-shaped domain, and a cube. On each domain, we consider the SIP, NIP, and IIIP methods.

5.3.1 Circular domain

In this test, we consider the unitary circle as computational domain, which we define by $\Omega_C := \{(x, y) \in \mathbb{R}^2 : x^2+y^2 \leq 1\}$. The relevance of this experiment is that we are approximating a curved domain with triangular meshes, which lead to a variational crime. As before, we consider the symmetric and nonsymmetric methods for this domain, and the results are reported for SIP, NIP, and IIP methods in Tables 14, 15, and 16, respectively. We mention that all the computed eigenvalues have been computed for $\mathtt{a} = 8$ and polynomial degrees $k = 1, 2, 3$ in each of the DG methods.

It is clear from Tables 14, 15, and 16 that for each DG method and for every polynomial degree, the order of convergence is $\mathcal{O}(h^2)$. These order of convergence are expectable due to the the variational crime committed when a curved domain is approximated with polygonal meshes (which in our case are meshes consisting in triangles). These results have been also observed in other formulations for the

Table 14 Smallest computed eigenvalues for polynomial degrees $k = 1, 2, 3$, $\mathtt{a} = 8$, and $\varepsilon = 1$

k	$N = 4$	$N = 8$	$N = 16$	$N = 32$	Order	λ_{extr}
1	15.8494	14.9674	14.7535	14.6999	2.04	14.6839
	29.9807	27.3034	26.6097	26.4337	1.95	26.3693
	29.9807	27.3034	26.6097	26.4337	1.95	26.3693
	50.2529	43.2118	41.3401	40.8653	1.92	40.6810
	50.2529	43.2118	41.3401	40.8653	1.92	40.6810
	59.2113	51.9202	49.9222	49.3980	1.88	49.1922
2	14.9900	14.7375	14.6939	14.6847	2.50	14.6835
	26.9900	26.4785	26.3962	26.3795	2.60	26.3780
	26.9890	26.4785	26.3962	26.3795	2.60	26.3780
	41.9030	40.8829	40.7408	40.7141	2.80	40.7130
	41.9030	40.8829	40.7408	40.7141	2.80	40.7130
	50.7293	49.4371	49.2603	49.2278	2.83	49.2268
3	14.8907	14.7285	14.6929	14.6846	2.18	14.6826
	26.7540	26.4582	26.3943	26.3793	2.19	26.3756
	26.7540	26.4582	26.3943	26.3793	2.19	26.3756
	41.3050	40.8358	40.7368	40.7137	2.23	40.7088
	41.3050	40.8358	40.7368	40.7137	2.23	40.7088
	49.9456	49.3750	49.2553	49.2273	2.23	49.2211

Table 15 Smallest computed eigenvalues for polynomial degrees $k = 1, 2, 3$, $\mathtt{a} = 8$, and $\varepsilon = -1$

k	$N = 4$	$N = 8$	$N = 16$	$N = 32$	Order	λ_{extr}
1	15.1752	14.7935	14.7097	14.6889	2.16	14.6841
	28.3699	26.8179	26.4826	26.4015	2.19	26.3835
	28.3699	26.8179	26.4826	26.4015	2.19	26.3835
	46.3610	41.9450	41.0018	40.7794	2.21	40.7297
	46.3610	41.9450	41.0018	40.7794	2.21	40.7297
	55.7968	50.6705	49.5649	49.3036	2.19	49.2397
2	15.2105	14.7898	14.7063	14.6877	2.31	14.6840
	27.4084	26.5935	26.4251	26.3867	2.26	26.3787
	27.4084	26.5935	26.4251	26.3867	2.26	26.3787
	42.6661	41.1105	40.7999	40.7290	2.30	40.7156
	42.6661	41.1105	40.7999	40.7290	2.30	40.7156
	51.5893	49.7150	49.3336	49.2462	2.27	49.2276
3	14.8772	14.7259	14.6925	14.6846	2.17	14.6827
	26.7505	26.4551	26.3937	26.3792	2.24	26.3761
	26.7505	26.4551	26.3937	26.3792	2.24	26.3761
	41.3482	40.8348	40.7362	40.7136	2.35	40.7100
	41.3482	40.8348	40.7362	40.7136	2.35	40.7100
	49.9642	49.3705	49.2541	49.2271	2.32	49.2225

Table 16 Smallest computed eigenvalues for polynomial degrees $k = 1, 2, 3$, $\mathtt{a} = 8$, and $\varepsilon = 0$

k	$N = 4$	$N = 8$	$N = 16$	$N = 32$	Order	λ_{extr}
1	15.4590	14.8634	14.7270	14.6932	2.11	14.6843
	29.0491	27.0132	26.5331	26.4142	2.07	26.3792
	29.0491	27.0132	26.5331	26.4142	2.07	26.3792
	48.0037	42.4555	41.1356	40.8131	2.07	40.7190
	48.0037	42.4555	41.1356	40.8131	2.07	40.7190
	57.2308	51.1762	49.7074	49.3410	2.04	49.2302
2	15.1067	14.7651	14.7004	14.6863	2.38	14.6840
	27.2123	26.5397	26.4115	26.3833	2.37	26.3787
	27.2123	26.5397	26.4115	26.3833	2.37	26.3787
	42.3108	41.0046	40.7723	40.7220	2.46	40.7156
	42.3108	41.0046	40.7723	40.7220	2.46	40.7156
	51.1920	49.5856	49.2994	49.2376	2.46	49.2298
3	14.8832	14.7270	14.6927	14.6846	2.17	14.6825
	26.7517	26.4564	26.3939	26.3793	2.22	26.3760
	26.7517	26.4564	26.3939	26.3793	2.22	26.3760
	41.3275	40.8351	40.7364	40.7136	2.29	40.7092
	41.3275	40.8351	40.7364	40.7136	2.29	40.7092
	49.9551	49.3724	49.2546	49.2272	2.28	49.2220

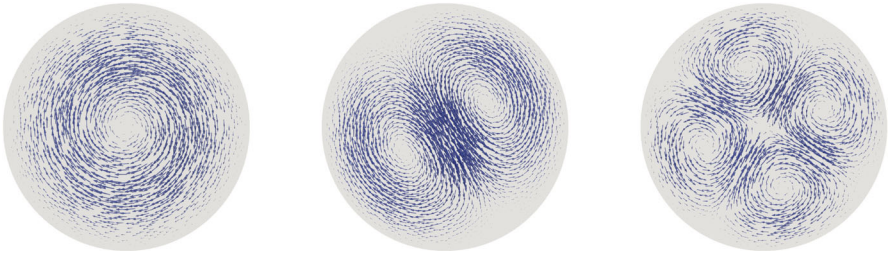

Fig. 6 Velocity fields associated with the first, second, and third eigenfunctions. These plots have been obtained with $\mathtt{a} = 10$, $N = 32$, and $k = 2$ for the IIP method

Stokes eigenproblem, as the primal pseudostress formulation of [17]. In Figs. 6 and 7 we present plots for the velocity fields and pressure fluctuation, respectively for the circular domain.

5.3.2 L-shape domain

In this numerical test, we consider an L-shape domain given by $\Omega := (-1, 1) \times (-1, 1) \backslash [-1, 0] \times [-1, 0]$. The order of convergence for the eigenvalues of this test is $1.7 \leq s \leq 2$ (see [19] for instance), where this fluctuation depends on the smoothness of the corresponding eigenfunctions.

For sake of simplicity, we present results for the lowest order polynomial approximation ($k = 1$). On Table 17 we present the computed eigenvalues on the L-shaped domain.

For this geometry, we observe that the results for SIP, NIP, and IIP are the expected. No complex eigenvalues were observed when the NIP and IIP methods are considered. Also, we observe that for the three methods, the order of convergence for the first eigenvalue is similar, due to the lack of smoothness of the associated eigenfunction. Finally, in Fig. 8, we present plots of the velocity fields, whereas in Fig. 9, we present pressure fluctuations on the L-shaped domain, both computed with the SIP method.

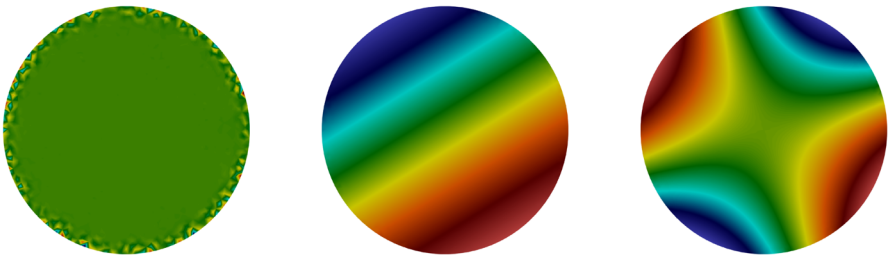

Fig. 7 Pressure fluctuation associated with the first, second, and fourth eigenfunctions. These plots have been obtained with $\mathtt{a} = 10$, $N = 32$, and $k = 2$ for the IIP method

Table 17 Smallest computed eigenvalues for polynomial degree $k = 1$, $\mathtt{a} = 8$, and $\varepsilon = 1$, $\varepsilon = -1$ and $\varepsilon = 0$, respectively

Method	$N = 12$	$N = 16$	$N = 20$	$N = 24$	$N = 28$	Order	λ_{extr}
SIP	35.0389	33.8121	33.3939	32.9322	32.7651	1.75	32.1046
	39.9709	38.4941	38.0245	37.7078	37.5065	2.50	37.2246
	45.9889	43.9096	43.2586	42.8401	42.5753	2.68	42.2343
	54.6011	51.9578	50.9847	50.2794	49.9092	2.15	49.0392
NIP	34.0110	33.2248	32.9082	32.6127	32.5480	1.84	32.1356
	39.0586	37.9569	37.6712	37.4868	37.3246	2.98	37.2234
	44.6660	43.2138	42.7825	42.5178	42.3335	2.84	42.1430
	52.7546	50.8729	50.2630	49.8289	49.5408	2.38	49.1056
IIP	34.0153	33.2267	32.9225	32.6196	32.5397	1.77	32.1007
	39.0557	37.9865	37.6850	37.4885	37.3325	2.80	37.1974
	44.6968	43.2560	42.8196	42.5363	42.3534	2.74	42.1374
	52.7985	50.9476	50.3094	49.8474	49.5773	2.26	49.0615

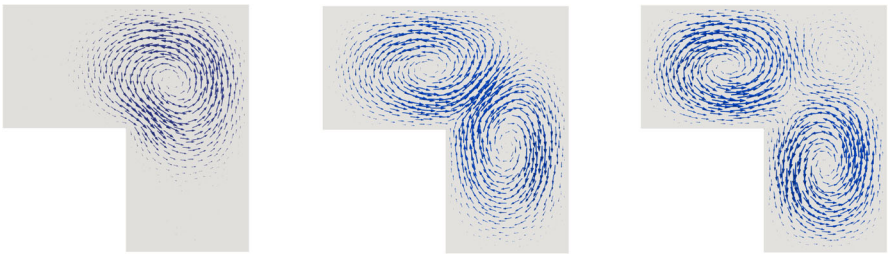

Fig. 8 Velocity fields associated with the first, second, and third eigenfunctions. These plots have been obtained with $\mathtt{a} = 10$, $N = 28$, and $k = 1$, for the SIP method

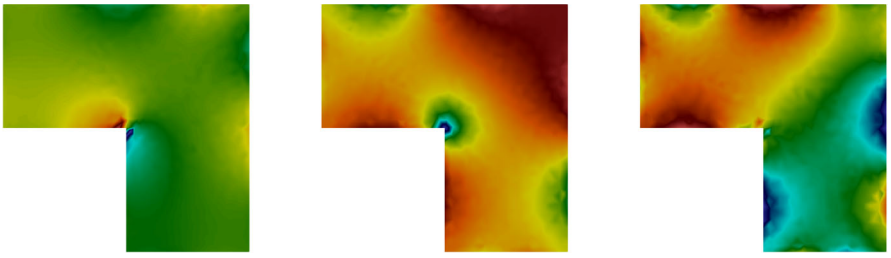

Fig. 9 Pressure fluctuation associated with the first, third, and fourth eigenfunctions. These plots have been obtained with $\mathtt{a} = 10$, $N = 28$, and $k = 1$, for the SIP method

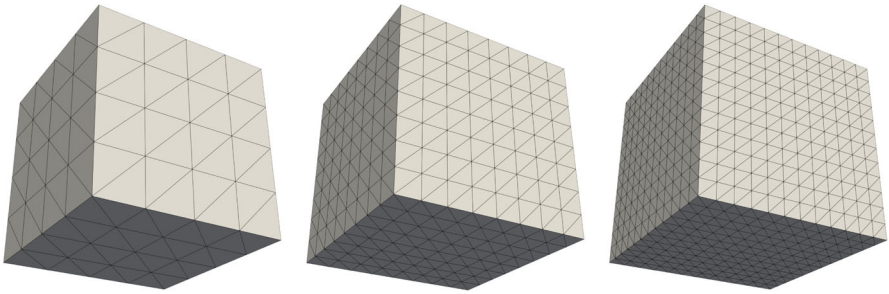

Fig. 10 Examples of the meshes used in the unit cube. The left figure represents a mesh for $N = 4$, the center figure for $N = 8$, and the right figure for $N = 12$

5.3.3 Cubic domain

In this test, we further assess the proposed schemes by consider a three-dimensional domain that consists on a cube defined by $\Omega = (0, 1)^3$. Here, N represents the number of cell per side such that the number of tetrahedron is $6(N+1)^3$. In Fig. 10, we present examples of the meshes used in the cube domain. We report, for simplicity, results for $k = 1$.

Table 18 Smallest computed eigenvalues for polynomial degree $k = 1$, $\mathtt{a} = 8$, and $\varepsilon = 1$, $\varepsilon = -1$ and $\varepsilon = 0$, respectively

Method	$N = 8$	$N = 10$	$N = 12$	$N = 14$	Order	λ_{extr}
SIP	64.8876	63.9227	63.3887	63.0640	1.92	62.1178
	65.7615	64.5206	63.8210	63.3899	1.84	62.0721
	65.7615	64.5206	63.8210	63.3899	1.84	62.0721
	97.8478	95.8009	94.6153	93.8668	1.70	91.3605
	97.8478	95.8009	94.6153	93.8668	1.70	91.3605
	101.5515	99.8105	98.7939	98.1556	1.68	95.9760
NIP	63.4782	62.9610	62.6975	62.5461	2.30	62.1906
	63.9410	63.2622	62.9081	62.7013	2.19	62.1859
	63.9410	63.2622	62.9081	62.7013	2.19	62.1859
	94.8467	93.6714	93.0361	92.6546	2.02	91.6089
	94.8467	93.6714	93.0361	92.6546	2.02	91.6089
	98.5714	97.6962	97.2347	96.9664	2.17	96.2883
IIP	63.8465	63.2119	62.8776	62.6808	2.15	62.1808
	64.4919	63.6407	63.1815	62.9068	2.04	62.1633
	64.4919	63.6407	63.1815	62.9068	2.04	62.1633
	95.6764	94.2720	93.4870	93.0033	1.86	91.5433
	95.6764	94.2720	93.4870	93.0033	1.86	91.5433
	99.3797	98.2708	97.6582	97.2891	1.94	96.2217

Table 18 reports the computed spectrum with the three methods considered in our work. We observe that for SIP, NIP, and IIP methods, the quadratic order is clear. In particular, for the SIP method, the order of convergence of the double eigenvalue $\lambda_3 = \lambda_4$ is lower compared with the rest of the eigenvalues, whereas for the NIP and IIP methods, the order $\mathcal{O}(h^2)$ is recovered with no problems.

Funding The first author has been partially supported by DICREA through project 2120173 GI/C Universidad del Bío-Bío and ANID-Chile through FONDECYT project 11200529, Chile.

Data Availability No datasets were generated or analysed during the current study.

Declarations

Conflict of interest The author declares no competing interests.

References

1. Antonietti, P.F., Buffa, A., Perugia, I.: Discontinuous Galerkin approximation of the Laplace eigenproblem. Comput. Methods Appl. Mech. Engrg. **195**, 3483–3503 (2006)
2. Arnold, D.N., Brezzi, F., Cockburn, B., Marini, L.D.: Unified analysis of discontinuous Galerkin methods for elliptic problems. SIAM J. Numer. Anal. **39**, 1749–1779 (2001)
3. Buffa, A., Houston, P., Perugia, I.: Discontinuous Galerkin computation of the Maxwell eigenvalues on simplicial meshes. J. Comput. Appl. Math. **204**, 317–333 (2007)
4. Buffa, A., Perugia, I.: Discontinuous Galerkin approximation of the Maxwell eigenproblem. SIAM J. Numer. Anal. **44**, 2198–2226 (2006)
5. Buffa, A., Perugia, I., Warburton, T.: The mortar-discontinuous Galerkin method for the 2D Maxwell eigenproblem. J. Sci. Comput. **40**, 86–114 (2009)
6. Descloux, J., Nassif, N., Rappaz, J.: On spectral approximation. I. The problem of convergence. Rairo Anal. Numér. **12**, 97–112 (1978)
7. Descloux, J., Nassif, N., Rappaz, J.: On spectral approximation. II. Error estimates for the Galerkin method. RAIRO Anal. Numér. **12**, 113–119 (1978)
8. Di Pietro, D.A., Ern, A.: Mathematical aspects of discontinuous Galerkin methods. Mathématiques & Applications (Berlin) [Mathematics & Applications], vol. 69. Springer, Heidelberg (2012)
9. Ern, A., Guermond, J.-L.: Theory and practice of finite elements. Applied Mathematical Sciences, vol. 159. Springer-Verlag, New York (2004)
10. Fabes, E.B., Kenig, C.E., Verchota, G.C.: The Dirichlet problem for the Stokes system on Lipschitz domains. Duke Math. J. **57**, 769–793 (1988)
11. Gardini, F.: Mixed approximation of eigenvalue problems: a superconvergence result. M2AN Math. Model. Numer. Anal. 43 (2009)
12. Gedicke, J., Khan, A.: Arnold-Winther mixed finite elements for Stokes eigenvalue problems. SIAM J. Sci. Comput. **40**, A3449–A3469 (2018)
13. Gedicke, J., Khan, A.: Divergence-conforming discontinuous Galerkin finite elements for Stokes eigenvalue problems. Numer. Math. **144**, 585–614 (2020)
14. Hansbo, P., Larson, M.G.: Discontinuous Galerkin methods for incompressible and nearly incompressible elasticity by Nitsche's method. Comput. Methods Appl. Mech. Engrg. **191**, 1895–1908 (2002)
15. Langtangen, H. P., Logg, A.: Solving PDEs in Python, vol. 3 of Simula SpringerBriefs on Computing, Springer, Cham, The FEniCS tutorial I (2016)
16. Lepe, F., Meddahi, S., Mora, D., Rodríguez, R.: Mixed discontinuous Galerkin approximation of the elasticity eigenproblem. Numer. Math. **142**, 749–786 (2019)
17. Lepe, F., Mora, D.: Symmetric and nonsymmetric discontinuous Galerkin methods for a pseudostress formulation of the Stokes spectral problem. SIAM J. Sci. Comput. **42**, A698–A722 (2020)
18. Lepe, F., Rivera, G., Vellojin, J.: Mixed methods for the velocity-pressure-pseudostress formulation of the Stokes eigenvalue problem. SIAM J. Sci. Comput. **44**, A1358–A1380 (2022)

19. Lovadina, C., Lyly, M., Stenberg, R.: A posteriori estimates for the Stokes eigenvalue problem. Numer. Methods Partial Differential Equ. **25**, 244–257 (2009)
20. Meddahi, S., Mora, D., Rodríguez, R.: A finite element analysis of a pseudostress formulation for the Stokes eigenvalue problem. IMA J. Numer. Anal. **35**, 749–766 (2015)
21. Savaré, G.: Regularity results for elliptic equations in Lipschitz domains. J. Funct. Anal. **152**, 176–201 (1998)